

1-D semi-analytical modeling and parametric study of a single phase rectangular Coupled Natural Circulation Loop

Akhil Dass, Sateesh Gedupudi ¹

Heat Transfer and Thermal Power Laboratory, Department of Mechanical Engineering, IIT Madras, Chennai 600036, India

Abstract

The study of heat exchangers with both the hot and cold fluid sides driven by buoyancy forces is an area of considerable interest due to their inherent passivity and non-existence of moving parts. The current study aims to study such heat exchange devices employing the basic Coupled Natural Circulation Loop (CNCL) systems. A 1-D Fourier series based semi-analytical model of the basic CNCL system is proposed. A 3-D CFD validation is performed to validate the developed 1-D model. The non-dimensional numbers such as Grashof number, Fourier number, Stanton number and Reynolds number, which determine the system behavior are identified and a detailed parametric study is performed. Both vertical and horizontal CNCL systems are considered along with the parallel and counter flow configurations. The heater-cooler location greatly influences the behavior of CNCL system. The vertical CNCL always exhibits counter flow configuration whereas the horizontal CNCL system may exhibit parallel or counter flow arrangement depending on the heater-cooler location and initial flow conditions.

Keywords: Natural Circulation Loop, 1D Mathematical model, Coupled system

1. Introduction

Heat exchange devices, also known as heat exchangers are heavily used in the industry and many daily life applications. The heat exchangers may be classified into various categories based on their size, geometry, and complexity. In the present study, the classification of heat exchangers based on the type of convection occurring on the hot and cold fluid sides is of prime interest. Figure 1 represents the flowchart of the aforementioned classification.

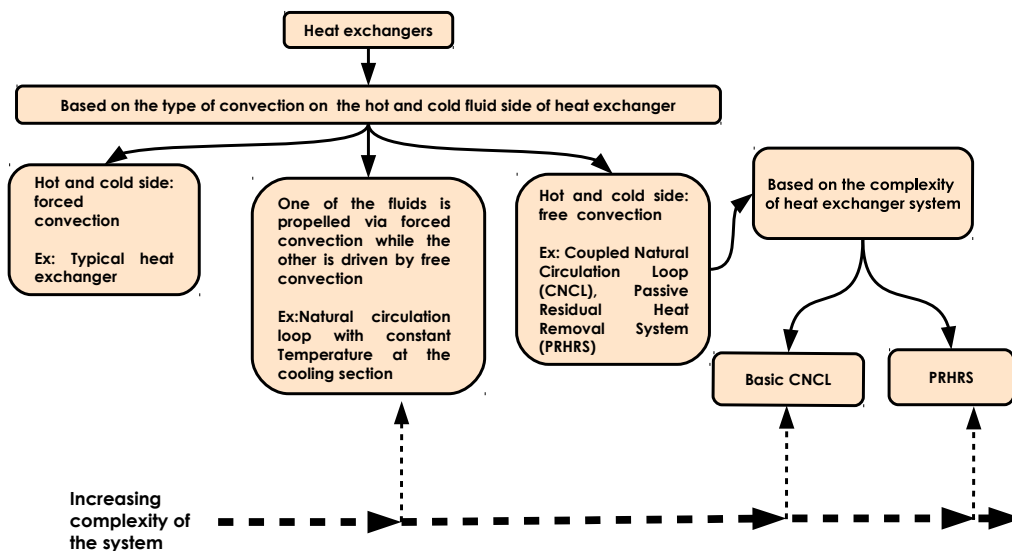


Figure 1: Classification of the heat exchangers based on the type of convection occurring at the hot and cold fluid sides.

¹Corresponding author. Tel.: +91 44 2257 4721, Email: sateeshg@iitm.ac.in

The study of typical heat exchangers with forced convection has been thoroughly performed and has become part and parcel of many engineering textbooks, whereas the study of heat exchangers with at least one of the fluids driven by buoyancy forces is still an area of active research interest. From Fig.1 we observe that a Natural Circulation Loop (NCL) , basic Coupled Natural Circulation Loop (CNCL) and Passive Residual Heat Removal Systems (PRHRS) are devices which employ buoyancy forces to initiate and maintain the flow. Natural circulation is a buoyancy-driven phenomenon that occurs in a closed conduit present in a body force field (gravitational, magnetic or centrifugal) when subjected to an external thermal stimulus.

A Natural Circulation Loop (NCL) is a device with circular or rectangular geometry that operates based on the natural circulation process when thermally stimulated at the heating and cooling sections (heat flux or internal heat generation or temperature boundary condition) of the loop, with the rest of the loop generally being insulated from the surroundings. The past five decades have witnessed a surge in the amount of literature pertaining to NCLs, which can directly be attributed to their applications in several domains such as solar heaters, turbine blade cooling, geothermal energy extraction, nuclear power generation, electronic chip cooling, chemical process industries, closed loop pulsating heat pipes, refrigeration, ship propulsion etc. [1].

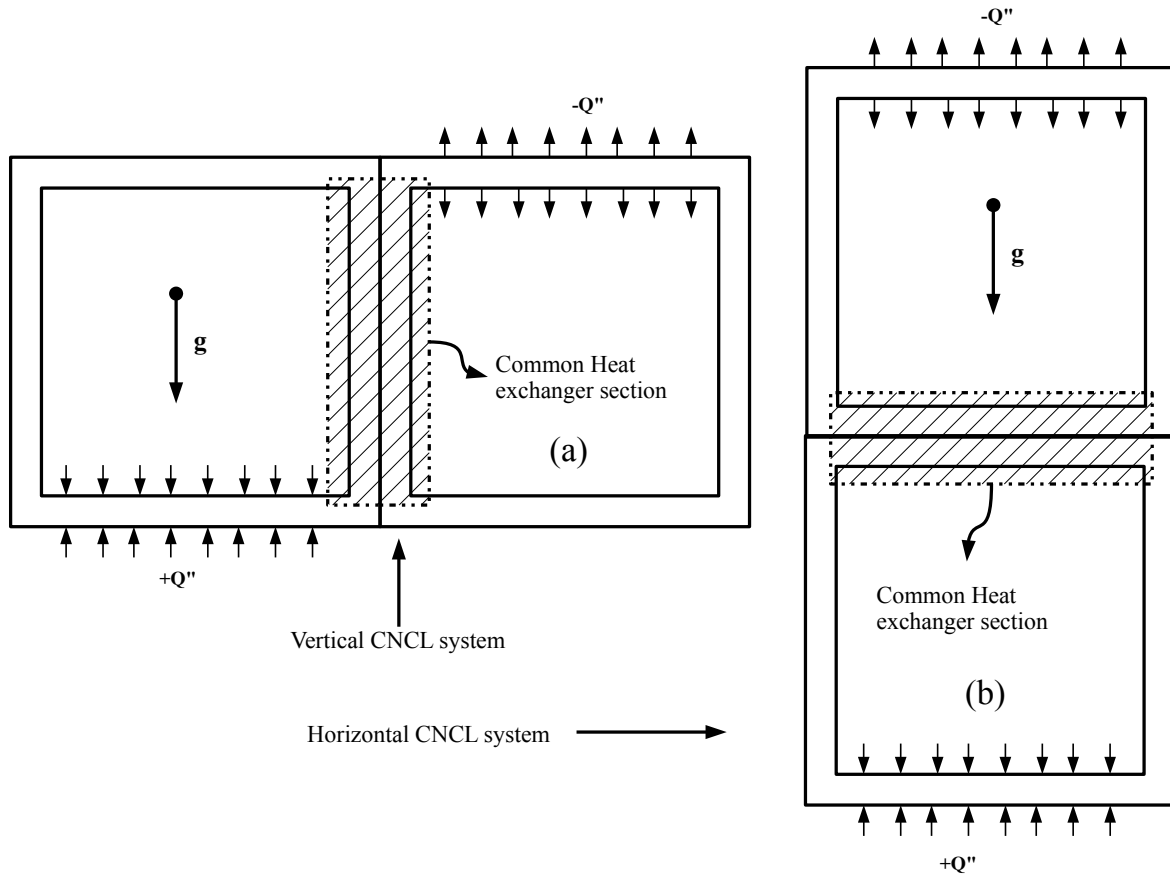


Figure 2: Basic CNCL systems considered for the current study. The CNCL systems are categorized as vertical or horizontal based on the common heat exchanger orientation w.r.t gravity.(a) Vertical CNCL system (b) Horizontal CNCL system.

Some general observations and characteristics of single-phase Natural Circulation Loops are listed below:

1. The NCL can be of any irregular geometry, but the toroidal and rectangular geometries have been extensively studied because of their simplicity and practical relevance [1].
2. The heater and cooler orientations influence the transient and steady-state behavior of the NCL [7].
3. The NCL is a dynamical system, which exhibits chaotic behavior at high power loads [8].

Table 1: Chronological summary of the literature pertaining to basic CNCL systems.

Si No	Year	Author	CNCL Geometry	Type of CNCL	Type of analysis	Method of analysis	Type of heat exchanger	Summary of salient points of the literature
1	1987	Davis and Roppo [2]	Toroidal	Vertical	Steady	1D analytical	Point contact	<ol style="list-style-type: none"> 1. Although the time dependent ODE system was presented no attempt was made to obtain the transient solution. 2. No validation of the model presented. 3. Primary focus on the stability of steady states.
2	1988	Ehrhard [3]	Toroidal	Vertical with square cross section	Transient and Steady	1D analytical and experimental	1D model-Point contact Experimental-Non point contact	<ol style="list-style-type: none"> 1. Experimental validation of the 1-D CNCL model developed by Davis and Roppo was performed employing bifurcation maps. 2. Transient validation of the 1-D model not performed.
3	1988	Salazar et al. [4]	Rectangular	Vertical	Steady	1D analytical	Flat plate	<ol style="list-style-type: none"> 1. Demonstrated the possibility of multiple steady state solution in rectangular CNCL. 2. No validation of the model was performed.
4	2015	Xun et al. [5]	Rectangular	Vertical	Transient	1D numerical and 2D CFD	Flat plate	<ol style="list-style-type: none"> 1. Validation of the 1-D numerical model with 2D CFD is performed. 2. Effect of heat transfer on oscillations of the CNCL is studied.
5	2016	Duffey and Hughes [6]	Rectangular	Vertical and Horizontal	Steady	1D analytical	General study	<ol style="list-style-type: none"> 1. Importance of the CNCL systems is presented. 2. The basic Horizontal and Vertical CNCL systems are depicted. 3. Links the basic CNCL and PRHRS.

4. The NCL system is also very sensitive to the initial conditions at high power loads [8].
5. The power supplied to the NCL determines its dynamic characteristics. For lower power inputs, the NCL reaches a steady state, while increasing the power input leads to flow pulsations and/or reversals [8].
6. The NCL has a Lorenz like attractor for higher power inputs [8].
7. The viscous and buoyancy forces dictate the dynamic behavior of the natural circulation system [9].

The above-mentioned characteristics and applications in numerous domains have augmented the research conducted

in the field of NCLs. The domain of interest of the current paper is the heat exchanger wherein both the hot and cold fluid sides are driven by buoyancy forces. A basic Coupled Natural Circulation Loop (CNCL) is an ideal device which can be used to investigate the characteristics of such systems. CNCL is a device that is constructed from two NCLs, which are coupled thermally via a common heat exchanger section. The component NCLs are not hydraulically linked; hence, the energy transfer between the two NCLs is solely due to thermal coupling at the heat exchanger section.

A considerable amount of literature has been published on the complex CNCL systems such as the PRHRS (both primary and secondary loops driven by buoyancy) but the literature pertaining to basic CNCL systems such as those represented by Fig.2 is limited. Table.1 represents the literature available on the basic CNCL systems.

Thus to add to the existing literature and provide a link between the NCL and PRHRS systems the following objectives are proposed for the present study:

1. Develop a 1-D semi-analytical mathematical model for the transient analysis of the basic rectangular CNCL system.
2. Conduct a 3-D CFD study of the basic rectangular CNCL system to validate the developed 1-D model and understand the behavior of systems represented in Fig.2.
3. Non-dimensionalize the 1-D model to identify the non-dimensional parameters which determine the CNCL behavior and thus by extension the PRHRS system.
4. Detailed parametric study of the CNCL system behavior by varying the non-dimensional numbers.
5. Study to determine the effect of heater and cooler configurations on the CNCL system behavior.
6. Study to determine the effect of parallel and counter flow orientations on the CNCL system response.
7. Study to determine the common heat exchanger orientation of a CNCL system w.r.t gravity.

The current study employs Fourier series to convert the Partial Differential Equations (PDE) of the CNCL system to Ordinary Differential Equations (ODE). Hart[10] was first to employ this method to toroidal NCL systems and truncate the terms to obtain the transient dynamics of the system. Davis and Roppo [2] utilized the methodology to model coupled toroidal NCLs and the point coupling was achieved by using the Dirac Delta function. Axial conduction effects were neglected in the models developed.

Bernal and Van Vleck [11] proposed a mathematical model for generic NCL geometry and incorporated the axial conduction effects of the fluid in the model. Fichera and Pagano [8] utilized this method to develop the model of a rectangular NCL with heat flux boundary conditions. They also validated the model against experimental results. The model of the rectangular NCL was capable of capturing both the steady and chaotic behavior of the NCL system. Salazar et al. [4] proposed a 1-D steady-state model of a generic CNCL system with non-point contact, but the axial conduction effects were not considered for the study. The existence of multiple steady-state solutions was attributed to the nonlinear convective term of the energy equation. A similar approach is utilized in the current paper to derive the transient PDE of the rectangular basic CNCL system.

The 1-D model developed in the paper incorporates the following effects, making the model more general:

- a) The axial conduction of the fluid is considered.
- b) The Fourier series is employed to model the geometry and boundary conditions.
- c) A non-point contact heat exchanger section is modeled.
- d) Transient behavior of the system can be computed after truncation of the infinite series.
- e) Bend loss effects are introduced in the model, which play a very vital role in the laminar regime.

Transient CFD studies on NCLs in the laminar regime have been conducted by Kudariyawar et al. [12] and Louisos et al [13]. Kudariyawar et al. performed transient CFD simulations using the laminar viscous model and observed that

there was a good agreement with the experimental data, the deviation observed in the initial phase of the transient trend may be attributed to the non-consideration of wall thickness. Louisos et al. performed 2D CFD simulations of the toroidal NCL in the laminar regime. The higher Rayleigh number ranges were achieved by modifying the gravity. It is observed from the literature that the time taken to approach steady state from transience for fluids such as water is of the order of 10^4 s, thus to minimize the time taken to reach steady state and also reduce the computational requirements fictitious fluids were chosen for the present study.

The paper begins with an introduction to the 1-D semi-analytical model of the CNCL, which includes governing equations, initial and boundary conditions and solution methodology. This is followed by a 3-D CFD study of the vertical and horizontal CNCL systems and validation of the 1-D CNCL model for all the CFD cases considered. Mesh and time step independence studies were performed and fictitious fluids were employed to reduce the computational load. The governing equations of the CNCL are non dimensionalized to obtain the non-dimensional numbers which characterize the CNCL system. This is followed by the results section which includes a detailed parametric study of the CNCL employing the non-dimensional numbers. Finally, conclusions are drawn from the study.

2. Contributions and benefits of the present study

1. It provides an analytical backbone to the study of basic CNCL systems: The current analysis provides an exact solution to the CNCL considered for the present study in terms of Fourier series, but because solving the resulting infinite dimensional system obtained is impractical, a truncated system is used with enough number of nodes to simulate the system dynamics.
2. The 1-D methodology developed can be used to model multiple coupled NCL systems with non-point area contact.
3. The method developed is extremely user-friendly, modifiable and does not require the use of any commercial software.
4. With extensions to the 1-D model developed in the current paper even complex systems may be modeled.
5. The stability analysis of the CNCL systems can be performed.

3. Mathematical modelling of CNCL system

Salazar et al. [4] were the first to perform a steady state analysis of the CNCL system with a flat plate heat exchanger. The following simplifications were incorporated by Salazar et al. to model the CNCL:

- a) The fluids in the primary and secondary loop of the CNCL are assumed to be driven exclusively via natural circulation.
- b) The Intermediate Heat Exchanger section of the CNCL is a flat plate heat exchanger.
- c) Heat transfer in the heat exchange zone is directly proportional to the local temperature difference between the primary loop and secondary loop.
- d) All thermophysical properties are assumed to have a constant magnitude.
- e) The Boussinesq hypothesis is employed to model the buoyancy forces.
- f) One dimensional NCL momentum and energy equations are used for the study.
- g) The axial heat conduction term of the energy equation is disregarded in the analysis performed.
- h) Frictional forces are considered to be a linear function of velocity.

The simplifications from (a) to (f) are considered in the present study with the inclusion of the axial heat conduction term and the implementation of a nonlinear function of velocity for the frictional forces. This study extends the analysis by enabling the modeling of the transient behavior of the CNCL system containing different fluids in each of the loops. Both Loop 1 and Loop 2 have identical dimensions and have a square cross-section. The current section only examines the 1-D modeling of Vertical CNCL, as the procedure is similar for the Horizontal CNCL configuration. To model the Horizontal CNCL, modifications are made to the piecewise functions representing the geometry and boundary conditions of the loops.

It is to be noted that employing the $-Q''$ on Loop 1 and $+Q''$ on Loop 2 at the CNCL common heat exchanger section results in a constant average temperature (w.r.t. time) in both loops thus decoupling the two loops. Hence the heat flux boundary condition cannot be employed at the common heat exchanger section, therefore a convection boundary condition is employed at the common heat exchanger section to model the CNCL system and ensure coupling amongst the constituent NCLs.

3.1. Governing equations of the CNCL

The CNCL has two NCLs: Loop 1, Loop 2, which are coupled at the common heat exchanger section. Corners of Loop 1 are denoted using alphabets (A-D) and that of Loop 2 are denoted using alphabets (E-H), as shown in Fig.3. To derive the governing equations of the CNCL system, the CNCL is divided into two parts. Thereby Loop 1 and Loop 2 become two distinct NCLs with the heat exchanger section transforming into the heat sink for the NCL formed by Loop 1 and heat source for the NCL formed by Loop 2. Figure 3 clearly depicts this process and labeling of the system. The objective behind flipping the NCL formed by Loop 1 vertically is to have a common sign for velocity vector (+ve in the clockwise direction) and have the origin O at the left bottom corner. Apart from the common heat exchanger section and limbs of the CNCL where the constant heat flux addition or removal condition is enforced, the rest of the CNCL is insulated from the surroundings.

The governing equations of the CNCL can be derived from the simple force and energy balance applied on an infinitesimal 1-D element of the constituent NCLs and using appropriate piecewise functions to represent the complete system.

The governing equations of the CNCL system are:

$$\rho_1 \frac{d\omega_1(t)}{dt} + \frac{4\tau_1}{D_h} = \frac{\rho_1 g \beta_1}{2(L + L1)} \left(\oint (T_1 - T_0) f_1(x) dx \right) - \frac{nK\rho_1\omega_1^2}{4(L + L1)} \quad (1)$$

$$\frac{\partial T_1}{\partial t} + \omega_1(t) \left(\frac{\partial T_1}{\partial x} \right) = H_1(x, t) + a_1 \frac{\partial^2 T_1}{\partial x^2} \quad (2)$$

$$\rho_2 \frac{d\omega_2(t)}{dt} + \frac{4\tau_2}{D_h} = \frac{\rho_2 g \beta_2}{2(L + L1)} \left(\oint (T_2 - T_0) f_2(x) dx \right) - \frac{nK\rho_2\omega_2^2}{4(L + L1)} \quad (3)$$

$$\frac{\partial T_2}{\partial t} + \omega_2(t) \left(\frac{\partial T_2}{\partial x} \right) = H_2(x, t) + a_2 \frac{\partial^2 T_2}{\partial x^2} \quad (4)$$

where,

$$\tau_1 = \frac{\rho_1 \omega_1^2 f_{F1}}{2} \quad (5)$$

$$\tau_2 = \frac{\rho_2 \omega_2^2 f_{F2}}{2} \quad (6)$$

Equations 1 and 3 represent the momentum equations of the Loop 1 and Loop 2, respectively. Equations 2 and 4 represent the energy equations of the Loop 1 and Loop 2, respectively. τ_1 and τ_2 represent the shear stresses acting

$f_i(x)$ is the function which represents the rectangular geometry of both Loop 1 and Loop 2. $\lambda(x)$ is the function which couples both Loop 1 and Loop 2.

3.2. Friction factor correlations

The frictional forces direct the dynamic behavior of the CNCL system; hence, it is pivotal to employ proper correlations to determine their magnitude as the flow develops with time. The current study involves flow in a square duct, thus the suitable friction factors for square duct are utilized. The general Fanning friction factor correlation is given by equation 11. In the laminar regime the magnitude of $C=14.23$ and $d=1$ for a square duct [14].

$$f_F = C/Re^d \quad (11)$$

3.3. Bend loss Correlations

The bend loss at the 90° elbow bends of the CNCL plays a very vital role in the transient evolution of the velocity and temperature distributions in the CNCL system. The bend loss coefficient (K) for the current study is evaluated using the 3K method. Equation (12) provides the expression of the 3K method bend loss correlation which is valid across the laminar, transition and turbulent regime [15]. The values of K_1, K_∞ and K_d used for elbow bend with $R/D_h = 1$ are 800, 0.14 and 4 respectively and D_n represents the hydraulic diameter of the elbow in inches [15].

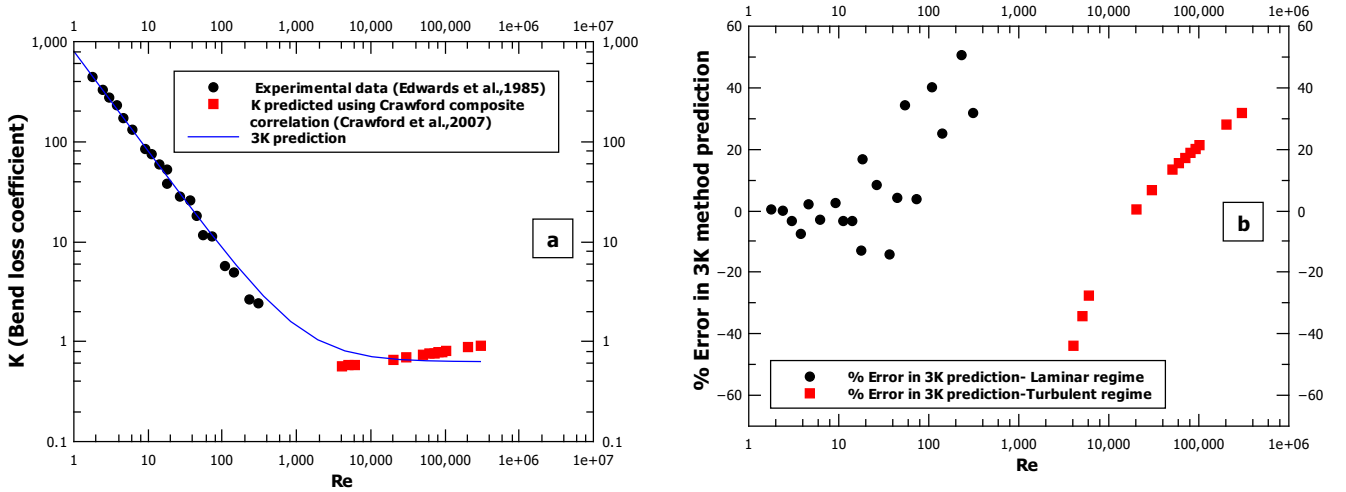


Figure 4: (a) Comparison of experimental data and 3K method prediction (b) Error introduced by the 3K method.

$$K = \frac{K_1}{Re} + K_\infty \left(1 + \frac{K_d}{D_n^{0.3}}\right) \quad (12)$$

Figure 4a compares the values of the 3K method prediction with experimental data. We observe that the 3K method provides a decent estimation of the bend loss over a wide range of Reynolds numbers. Figure 4b represents the corresponding error of the 3K method prediction with experimental data. We observe that the maximum error associated with the 3K prediction is roughly $\pm 50\%$. The experimental bend loss data in laminar regime was taken from the work of Edwards et al.[16] and the data for the turbulent regime was obtained employing the Crawford composite correlation from the work of Crawford et al.[17].

3.4. Initial and boundary conditions of the CNCL system

3.4.1. Initial conditions

The initial condition of the CNCL system is represented by the initial conditions of Loop 1 and Loop 2. The initial conditions for the momentum and energy equations of the CNCL system are depicted by equations 13 and 14.

$$w_1(0) = w_0, \quad w_2(0) = w_0 \quad (13)$$

$$T_1(x, 0) = T_0, \quad T_2(x, 0) = T_0 \quad (14)$$

3.4.2. Boundary conditions

$h_1(x)$ is the function which represents the location of the positive heat flux boundary condition of Loop 1. $h_2(x)$ is the function which represents the location of the negative heat flux boundary condition of Loop 2.

$$h_1(x) = \begin{cases} 0 & 0 < x < L \\ 0 & L < x < L + L1 \\ 0 & L + L1 < x < 2L + L1 \\ \left(\frac{4Q''}{\rho_1 C_{p,1} D_h} \right) & 2L + L1 < x < 2(L + L1) \end{cases} \quad (15)$$

$$h_2(x) = \begin{cases} 0 & 0 < x < L \\ \left(\frac{-4Q''}{\rho_2 C_{p,2} D_h} \right) & L < x < L + L1 \\ 0 & L + L1 < x < 2L + L1 \\ 0 & 2L + L1 < x < 2(L + L1) \end{cases} \quad (16)$$

3.5. ODEs which represent the 1-D single phase CNCL system

To simplify the task of obtaining the solution to the aforementioned (Equation 2 and Equation 4) partial differential equations (PDEs), we employ the Fourier series expansions of the temperature and boundary conditions to convert the PDEs to ordinary differential equations (ODEs).

$$T_1(x, t) = \sum_{k=-\infty}^{\infty} \alpha_k(t) e^{ik\pi x/(L+L1)} \quad (17)$$

$$T_2(x, t) = \sum_{k=-\infty}^{\infty} \beta_k(t) e^{ik\pi x/(L+L1)} \quad (18)$$

$$h_1(x) = \sum_{k=-\infty}^{\infty} \gamma_k e^{ik\pi x/(L+L1)} \quad (19)$$

$$h_2(x) = \sum_{k=-\infty}^{\infty} \delta_k e^{ik\pi x/(L+L1)} \quad (20)$$

$$\lambda(x) = \sum_{k=-\infty}^{\infty} \zeta_k e^{ik\pi x/(L+L1)} \quad (21)$$

$$f(x) = \sum_{k=-\infty}^{\infty} A_k e^{ik\pi x/(L+L1)} \quad (22)$$

where,

$$\alpha_0(t) = \frac{1}{2(L+L1)} \int_0^{2(L+L1)} T_1(x, t) dx \quad (23)$$

$$\beta_0(t) = \frac{1}{2(L+L1)} \int_0^{2(L+L1)} T_2(x, t) dx \quad (24)$$

for all t . In addition $\overline{\alpha_k} = \alpha_{-k}$, the same applies for all aforementioned complex Fourier coefficients.

Substituting the above expressions in equations (1-4) results in the following set of equations after restricting the number of Fourier nodes to three:

$$\frac{d\omega_1(t)}{dt} + \frac{2C}{D_h} \left(\frac{\nu}{D_h}\right)^d (\omega_1)^{2-d} = g\beta \sum_{n=-3}^3 \alpha_n A_{-n} - \frac{nK\omega_1^2}{4(L+L1)} \quad (25)$$

$$\frac{d(\alpha_0(t))}{dt} + = \gamma_0 - \sum_{n=-3}^3 \frac{U}{\rho_1 C_{p1} D_h} \zeta_{-n} (\alpha_n(t) - \beta_n(t)) \quad (26)$$

$$\frac{d(\alpha_1(t))}{dt} + \frac{i\pi}{L+L1} w_1(t) \alpha_1(t) = \gamma_1 - \frac{a\alpha_1(t)\pi^2}{(L+L1)^2} - \sum_{n=-3}^3 \frac{U}{\rho_1 C_{p1} D_h} \zeta_{1-n} (\alpha_n(t) - \beta_n(t)) \quad (27)$$

$$\frac{d(\alpha_2(t))}{dt} + \frac{2i\pi}{L+L1} w_1(t) \alpha_2(t) = \gamma_2 - \frac{4a\alpha_2(t)\pi^2}{(L+L1)^2} - \sum_{n=-3}^3 \frac{U}{\rho_1 C_{p1} D_h} \zeta_{2-n} (\alpha_n(t) - \beta_n(t)) \quad (28)$$

$$\frac{d(\alpha_3(t))}{dt} + \frac{3i\pi}{L+L1} w_1(t) \alpha_3(t) = \gamma_3 - \frac{9a\alpha_3(t)\pi^2}{(L+L1)^2} - \sum_{n=-3}^3 \frac{U}{\rho_1 C_{p1} D_h} \zeta_{3-n} (\alpha_n(t) - \beta_n(t)) \quad (29)$$

$$\frac{d\omega_2(t)}{dt} + \frac{2C}{D_h} \left(\frac{\nu}{D_h}\right)^d (\omega_2)^{2-d} = g\beta \sum_{n=-3}^3 \beta_n A_{-n} - \frac{nK\omega_2^2}{4(L+L1)} \quad (30)$$

$$\frac{d(\beta_0(t))}{dt} = \delta_0 + \sum_{n=-3}^3 \frac{U}{\rho_2 C_{p2} D_h} \zeta_{-n} (\alpha_n(t) - \beta_n(t)) \quad (31)$$

$$\frac{d(\beta_1(t))}{dt} + \frac{i\pi}{L+L1} w_2(t) \beta_1(t) = \delta_1 - \frac{a\beta_1(t)\pi^2}{(L+L1)^2} + \sum_{n=-3}^3 \frac{U}{\rho_2 C_{p2} D_h} \zeta_{1-n} (\alpha_n(t) - \beta_n(t)) \quad (32)$$

$$\frac{d(\beta_2(t))}{dt} + \frac{2i\pi}{L+L1} w_2(t) \beta_2(t) = \delta_2 - \frac{4a\beta_2(t)\pi^2}{(L+L1)^2} + \sum_{n=-3}^3 \frac{U}{\rho_2 C_{p2} D_h} \zeta_{2-n} (\alpha_n(t) - \beta_n(t)) \quad (33)$$

$$\frac{d(\beta_3(t))}{dt} + \frac{3i\pi}{L+L1} w_2(t) \beta_3(t) = \delta_3 - \frac{9a\beta_3(t)\pi^2}{(L+L1)^2} + \sum_{n=-3}^3 \frac{U}{\rho_2 C_{p2} D_h} \zeta_{3-n} (\alpha_n(t) - \beta_n(t)) \quad (34)$$

The equations [27-29] and [32-34] are separated into real and imaginary parts, thereby obtaining a set of 16 ordinary differential equations which need to be solved simultaneously to obtain $T_1(x, t)$ and $T_2(x, t)$. The Fourier coefficients are plugged into equations [35,36] to obtain temperature distributions in Loop 1 and Loop 2.

$$T_1(x, t) = \sum_{k=-3}^3 \alpha_k(t) e^{ik\pi x/(L+L1)} \quad (35)$$

$$T_2(x, t) = \sum_{k=-3}^3 \beta_k(t) e^{ik\pi x/(L+L1)} \quad (36)$$

3.6. Initial conditions of the ODE system

To obtain the transient behavior of the CNCL system we need to integrate the ODEs represented by equations (25-34) for which the initial conditions for each of the Fourier nodes need to be determined. The initial conditions of the ODEs are derived from the initial conditions of the momentum and energy equation for both Loop 1 and Loop 2. Since the number of nodes is limited to three, we place the nodes equidistantly along the loop and apply the initial conditions mentioned in equations (13) and (14). This results in a matrix of 4 equations and 4 unknowns for each of the loops, as represented below.

$$\begin{bmatrix} 1 & 1 & 1 & 1 \\ 1 & e^{i2\pi/3} & e^{i4\pi/3} & e^{i6\pi/3} \\ 1 & e^{i4\pi/3} & e^{i8\pi/3} & e^{i12\pi/3} \\ 1 & e^{i6\pi/3} & e^{i12\pi/3} & e^{i18\pi/3} \end{bmatrix} \times \begin{bmatrix} \alpha_0 \\ \alpha_1 \\ \alpha_2 \\ \alpha_3 \end{bmatrix} = \begin{bmatrix} T_0 \\ T_0 \\ T_0 \\ T_0 \end{bmatrix}$$

$$\begin{bmatrix} 1 & 1 & 1 & 1 \\ 1 & e^{i2\pi/3} & e^{i4\pi/3} & e^{i6\pi/3} \\ 1 & e^{i4\pi/3} & e^{i8\pi/3} & e^{i12\pi/3} \\ 1 & e^{i6\pi/3} & e^{i12\pi/3} & e^{i18\pi/3} \end{bmatrix} \times \begin{bmatrix} \beta_0 \\ \beta_1 \\ \beta_2 \\ \beta_3 \end{bmatrix} = \begin{bmatrix} T_0 \\ T_0 \\ T_0 \\ T_0 \end{bmatrix}$$

Solving the matrix equations yields the initial value of the Fourier nodes of Temperature. The solution is $\alpha_0 = \beta_0 = T_0$, whilst the values at all other nodes is zero.

3.7. Numerical integration

The set of ODEs obtained by using the Fourier series expansion cannot be solved analytically. Thus to obtain the dynamics of the system we need to use numerical integration techniques such as the Runge-Kutta method which has been employed for the current study using the MATLAB solver 'ode45'.

4. 3-dimensional CFD study of a single phase CNCL system

A detailed CFD investigation of the single-phase CNCL system has been conducted to explore the physics and dynamic characteristics. The main objective of this CFD study is to validate the 1-D CNCL model rigorously and probe its efficacy. The 3-D CFD study has been performed to study the single-phase CNCL system for the set of conditions specified in Table.2.

Table 2: Cases considered for the CFD simulation.

Case	Loop 1	Loop 2	CNCL Orientation	Description
CNCL-(a)	FF1	FF1	Vertical	Same fluid in both loops with counter flow configuration
CNCL-(b)	FF1	FF2	Vertical	Different fluids in the loops with counter flow configuration
CNCL-(c)	FF1	FF1	Horizontal	Same fluid in both loops with parallel flow configuration
CNCL-(d)	FF1	FF1	Horizontal	Same fluid in both loops with counter flow configuration

The developed 1-D model has been validated with the aforementioned CFD cases to display its robustness for use in prediction of the behavior of CNCL system. The CFD investigation of the CNCL system has been done using ANSYS Fluent, which is a commercial finite volume software. The pre-processing, processing and post-processing were performed employing the same software. FF1 and FF2 listed in Table.2 are the fluids used in this study, the thermophysical properties of which are elaborated in section 4.3.1.

4.1. Geometry

The geometry comprises of two parts: Loop 1 and Loop 2 which are coupled at the common heat exchanger section (flat plate heat exchanger). Loop 1 & 2 are square NCLs with a square cross-sectional area. Figure 5 represents the CNCL geometry considered for the study. The 90-degree bends are chamfered to reduce the bend losses encountered by the flow. Apart from the cooling and heating sections, the rest of the loop is completely insulated. The dimensions of the geometry considered for the study are listed in Table.3.

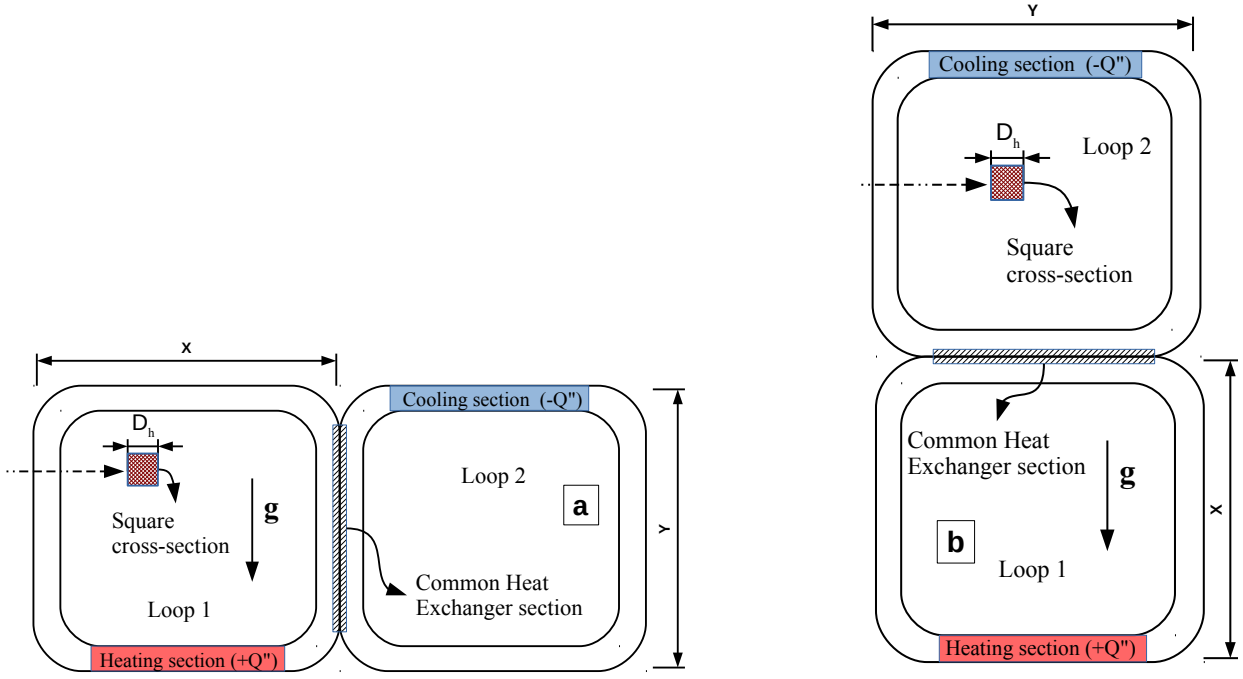


Figure 5: Schematic of the CNCL geometry made of square NCLs Loops 1 and 2 with a square cross section considered for CFD study. (a) Geometry of vertical CNCL cases CNCL-(a) and CNCL-(b). (b) Geometry of horizontal CNCL cases CNCL-(c) and CNCL-(d).

Table 3: Dimensions of the 3-D geometry

Parameter	Description	Dimensions
X	Height/Width of the CNCL	1 m
Y	Height/Width of the CNCL	1 m
D_h	Length of square cross section	0.04 m

4.2. Meshing

The ANSYS Design Modeler was used to generate a structured 3-D mesh from the geometry, as shown in Fig.6. The Multi-zone method was used along with the body sizing option to generate a hex-dominant high-quality mesh. Two meshes are considered, one without inflation called as Mesh-A and one with inflation as Mesh-B.

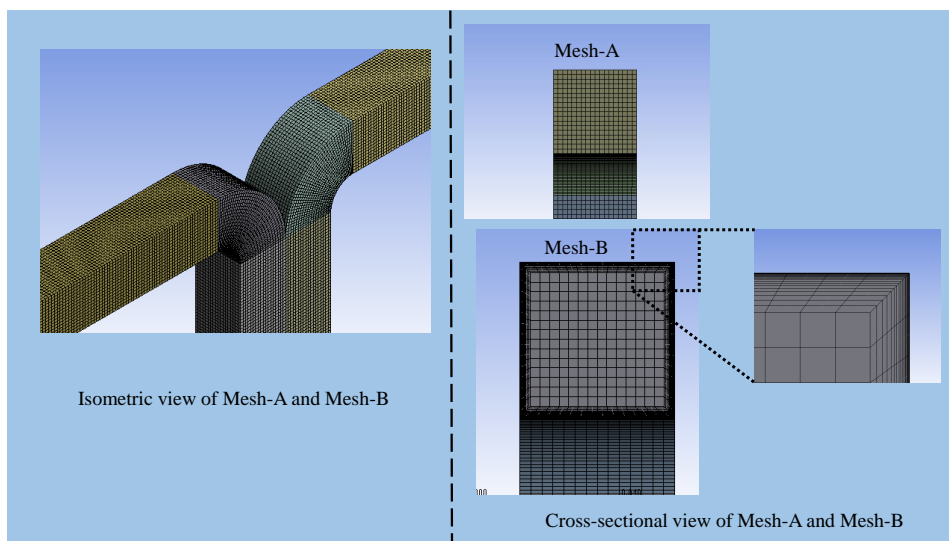


Figure 6: Schematic of the mesh used for the CFD study. Mesh-A represents the mesh without inflation at the walls and Mesh-B represents the mesh with inflation.

4.3. Case setup

A transient pressure based solver was used to simulate the transient dynamics of the CNCL system considered. The energy and momentum equation were solved simultaneously on the 3-D grid to obtain the numerical solution at each time step. The laminar flow model was used for the current simulation with the gravity set to 9.81 m/s^2 .

The Boussinesq approximation has been used to model the buoyancy forces. The operating temperature at startup is set to 300 K and the operating pressure is set to 1 atm .

4.3.1. Fluids used for the CFD study

It is observed that the fluids which are normally used, have very low values of thermal diffusivity. This becomes an issue when one tries to numerically solve the coupled momentum and energy equations of buoyancy-driven flows. The low values of thermal diffusivity impose the selection of an extremely fine mesh and a small time step to get a numerically stable CFD solution. Thus if we employ common fluids such as water, for a given heat input they might require about 50 min to reach the steady state ([8]). Besides, the extremely fine mesh and minute time step requirements make the computational process extremely expensive both in terms of memory and in terms of the clock time if we simulate until the fluid reaches a steady state. Since one of the main objectives is to validate the 1-D semi-analytical model developed we employ a fictitious fluid (a fluid with assumed thermophysical properties) for the 3-D CFD simulations to relax the mesh and time step conditions for numerical stability and hasten the time required to reach the steady state. The fluid chosen for simulation must be irrelevant as long as the underlying physics is the same. The thermophysical properties of the fictitious fluids are listed in Table.4.

Table 4: Fluids used for the CFD study.

Property	Fictitious fluid 1 (FF1)	Fictitious fluid 2 (FF2)
ρ_0	70 kg/m^3	50 kg/m^3
C_p	100 J/kgK	70 J/kgK
β	0.01 1/K	0.08 1/K
a	$0.4 \text{ m}^2/\text{s}$	$0.8 \text{ m}^2/\text{s}$
μ	0.0007 kg/ms	0.005 kg/ms

4.3.2. Initial and boundary conditions

At time $t = 0$ the operating temperature is T_0 and the operating pressure is P_0 . Apart from the heating, cooling and coupled heat exchanging section, the rest of the loop is completely insulated. We apply a constant heat flux Q'' at the heating section and the corresponding negative value at the cooling section. The coupling that was done in the geometry section results in the formation of a shadow for the coupled wall region. Table.5 lists the initial and boundary conditions of the CFD system used for the current simulation for all the cases CNCL-(a) to CNCL-(d) mentioned in Table.2.

Table 5: Initial and boundary conditions

Parameter	Description	Values
T_0	Temperature at time $t = 0$	300 K
P_0	Pressure at time $t = 0$	1 atm
Q''	Constant heat flux supplied or extracted	2000 W/m^2
g	Gravitational constant	9.81 m/s^2

4.3.3. Solver settings and discretization schemes

The PISO scheme was used for pressure-velocity coupling. The least squares cell-based scheme was used for the gradient spatial discretization. A second-order scheme for pressure discretization and second-order upwind scheme for the momentum and energy discretization was used respectively. Default solution controls with residuals of the order 10^{-3} were used and the average velocity and temperature were used as parameters for judging the convergence. The velocity field was initialized to zero and the temperature in the entire domain at time $t = 0$ s was set to 300 K. A fixed time stepping method was used and the number of iterations per time step was set to 200.

4.4. Grid independence and time step independence tests

To confirm the reliability of the results obtained, grid and time step independence tests were performed to ensure that the spatial and temporal discretization errors have a minimal impact on the physics of the study. Figures 7a and 7b represent the time step and grid independence results, respectively. The tests are considered to be satisfactory when percentage error is less than 5%. From the tests, it is observed that a time step of '1s' and Mesh A with no of elements '= 520968' to be ideal for CFD study for the case when both the loops of the CNCL are filled with FF1. We observe that introducing inflation (Mesh B) has not much effect on the transient behavior, indicating that Mesh A captures all the essential physics of the problem considered. The grid and time step studies were performed for all the cases used for validation with the 1-D semi-analytical model.

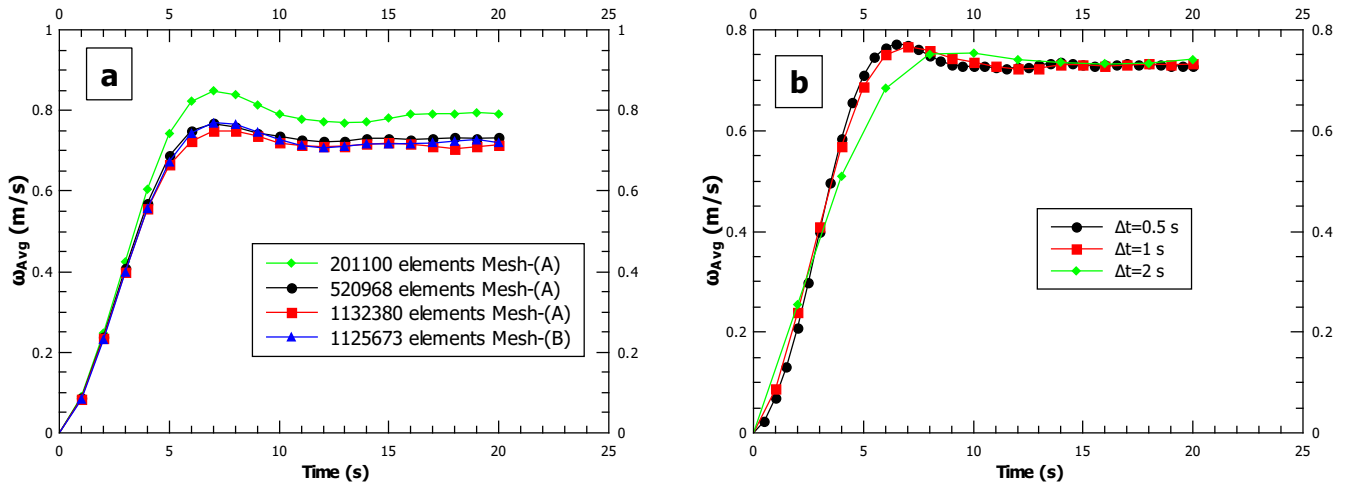


Figure 7: Reliability evaluation of the CFD simulation employing grid and time step independence tests.(a) Grid independence test (b) Time step independence test.

4.5. Flow model selection

The CFD simulations undertaken for the cases CNCL-(a) to CNCL-(d) for the given boundary conditions results in a maximum Reynolds number of ≈ 3000 (corresponding to 0.73 m/s for CNCL-(a) and 0.79 m/s for CNCL-(d)), thus to ensure the validity of selection of the laminar model it is compared with other turbulence models which take care of the transition from laminar to turbulence. From Fig.8 we can clearly see that there is a good agreement ($\pm 7\%$) among all the flow models considered. Thus from this study one can clearly note that laminar flow model is ideal for capturing the transient dynamics of natural circulation systems which transition across different flow regimes and is in good agreement ($\pm 5\%$) with the Spalart-Allmaras turbulence model for the considered cases. Thus the laminar flow model is considered for all the CFD cases for a maximum Reynolds number of approximately 3000 as the transition effects are minimal.

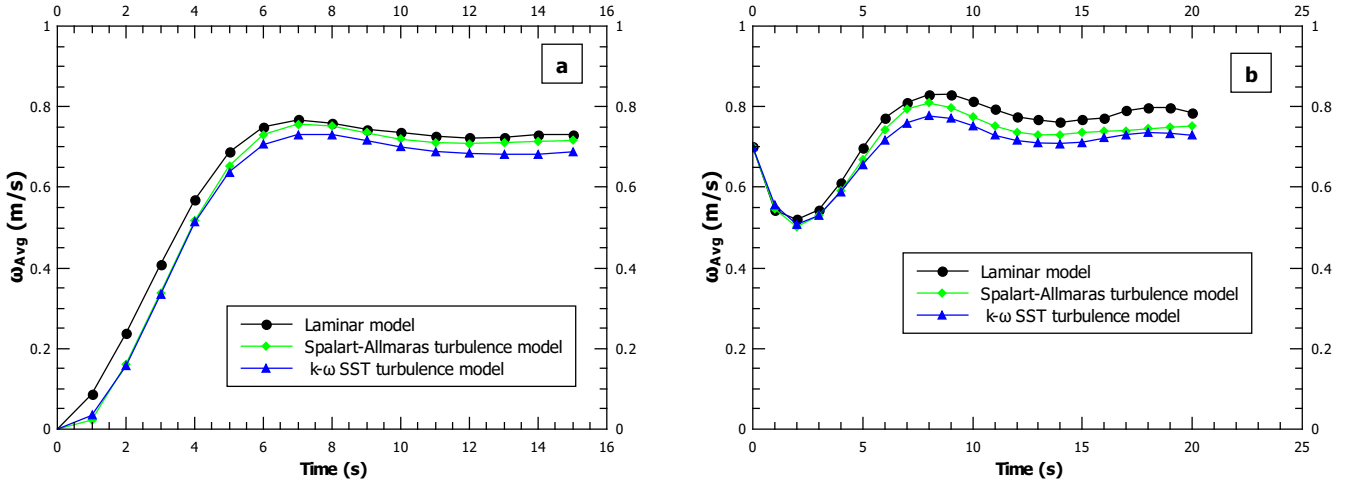


Figure 8: : Effect of different viscosity models on the CNCL system dynamics for a maximum Reynolds number of 3000 . (a) Flow model comparison for vertical CNCL for $Re = 2920$ (b) Flow model comparison for horizontal CNCL for $Re = 3160$.

5. CFD results and analysis

This section provides the validation of the CFD methodology and a brief discussion of the 3-D CFD simulation of the horizontal and vertical CNCL systems. The heat transfer and transient dynamics observed in the CNCL systems are governed by coupled velocity and temperature fields of each of its constituent NCLs as observed in equations (1-4) along with the thermal coupling in the heat exchanger section of the CNCL. Thus the velocity and temperature distribution in both Loop 1 and Loop 2 need to be studied to characterize a CNCL system.

5.1. Validation of the CFD methodology

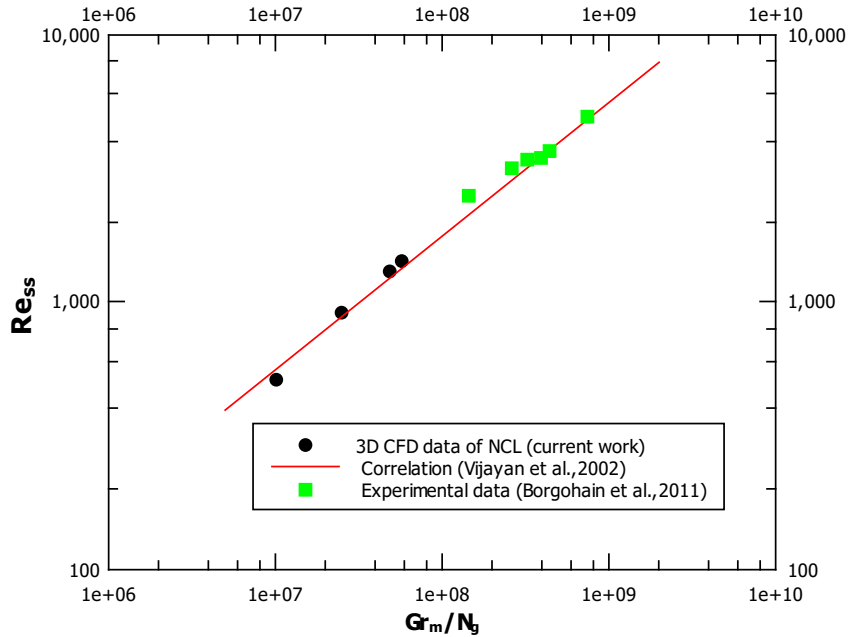


Figure 9: Validation of the CFD methodology with correlation and experimental data.

The validation of the CFD methodology is performed by considering an NCL with horizontal heater and cooler sections and having the same geometry as Loop 1 of case CNCL-(a). The CFD simulation is carried out using the same settings and flow models described in section.4. Figure 9 indicates an excellent agreement between the CFD

simulations and the previous literature, thus successfully validating the CFD study performed. The experimental data is taken from Borgohain et al. [18] and the correlation proposed by Vijayan [19] for the steady state Reynolds number as a function of Gr_m/N_g for an NCL is given as :

$$Re_{ss} = 0.1768 \left(\frac{Gr_m}{N_g} \right)^{0.5} \quad (37)$$

the definitions of Gr_m and N_g can be found in [19].

5.2. Steady state velocity and temperature contours

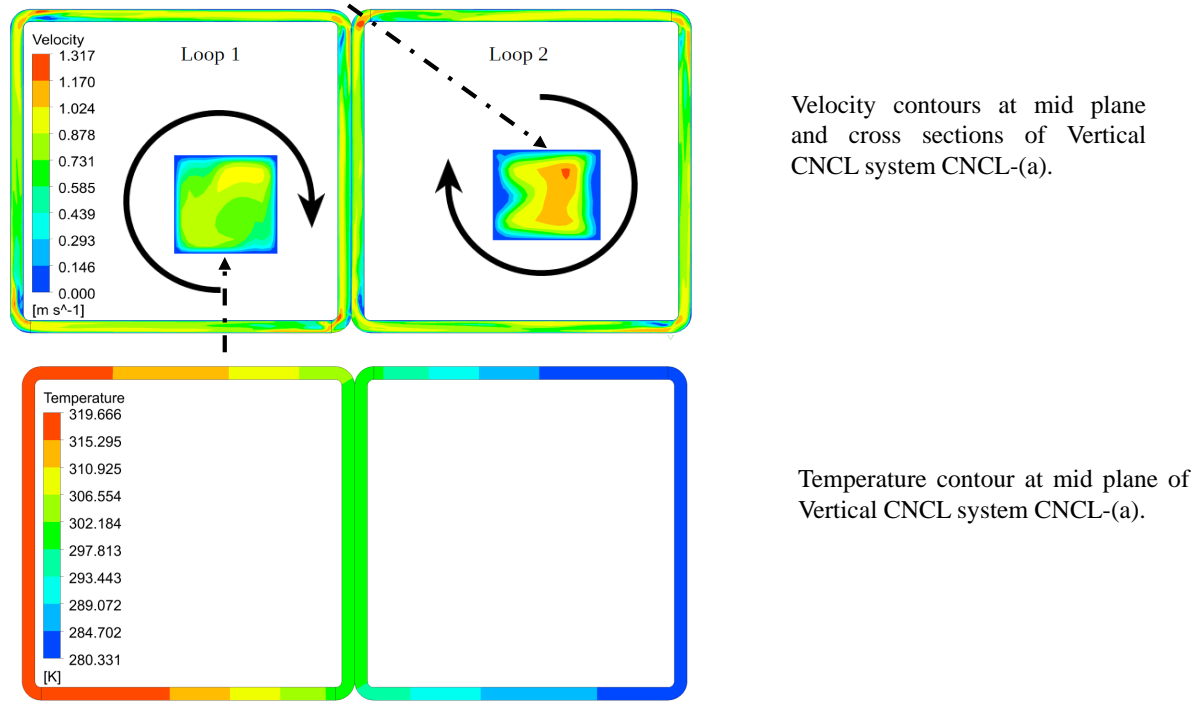


Figure 10: Steady state contours of vertical CNCL considered for study with both the loops containing FF1.

The velocity and temperature contours at steady state are illustrated in Fig.10. The velocity of the loop is uniform across the entire domain at the mid-plane except near the bends of the CNCL where the velocity magnitude is relatively lower. This indicates that the 90 ° elbow bends have a significant impact on the flow. We also observe that the temperature drop or rise occurs only along the direction of flow, with very little radial variation in the temperature profile. This is mainly due to the high thermal conductivity of the fluid considered for the study.

From the velocity contours of the cross-section of Loop 1 and Loop 2 we observe that the velocity is zero at the walls and gradually becomes higher in magnitude at the center, while the peculiar distribution of velocity observed in cross-section contour of Loop 2 is because of the centrifugal forces acting upon on the fluid at the 90° smooth elbow bend.

5.3. Transient dynamics of the CNCL system

Average velocity and average temperature are utilized as parameters to compare the 3-D CFD case with the 1-D semi-analytical model. These parameters are averaged over the volume of the respective NCLs, which make up the CNCL system. Figure 11 represents the CFD data obtained from the 3-D simulation of the CNCL system for cases CNCL-(a) to CNCL-(d).

From Fig.11 the following observations can be made:

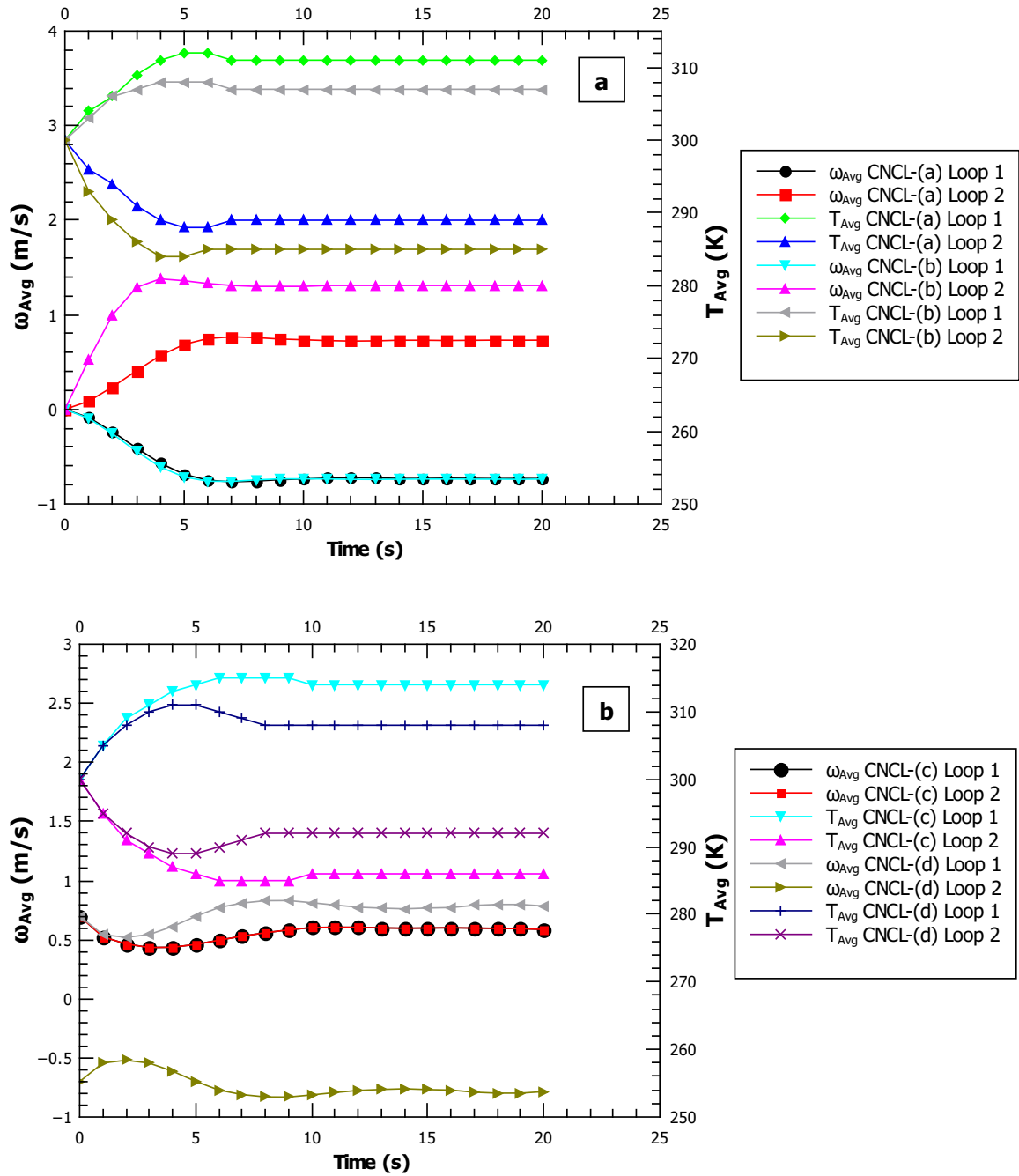


Figure 11: Transient volume averaged plots of velocity and temperature of the vertical and horizontal CNCL system obtained using CFD. (a) Vertical CNCL transient plot (b) Horizontal CNCL transient plot.

1. The introduction of a different fluid in one of the loops(as in the case of CNCL-(b)) does not seem to affect the transient average velocity plot of the other loop, but the transient temperature plot is influenced significantly as observed from Fig.11a which compares CNCL-(a) and CNCL-(b).
2. When both loops contain the same fluid the average transient temperature plot is symmetric about T_0 (which is the initial value of the average temperature of the constituent loops of the CNCL system), but when a different fluid (as in the case of CNCL-(b)) is introduced in one of the loops this symmetry is lost.
3. From Fig.11b (horizontal CNCL system) we observe that when both the loops are initiated with a certain velocity, depending on the direction of velocity in each of the loops the flow can either be in counter-flow(CNCL-(d)) or parallel-flow configuration(CNCL-(c)). The counter-flow configuration has a greater velocity magnitude in comparison with the parallel-flow configuration for the horizontal CNCL system. The cause behind this effect is

elaborated in section 8.2.

- For horizontal CNCL, the average temperature of the counter-flow configuration is lower in magnitude than the parallel-flow configuration. This is because of the uniform temperature drop along the length of the heat exchanger section for the counter-flow arrangement in contrast with the parallel-flow arrangement.

The steady state overall heat transfer coefficient (U) obtained from CFD simulations for cases CNCL-(a) to CNCL-(c) is about $\approx 19000 W/m^2K$ and for CNCL-(d) it is about $\approx 29000 W/m^2K$. For the counter flow case (CNCL-(d)) the magnitude of overall heat transfer coefficient is larger due to higher magnitude of velocity at the steady state in comparison with the parallel flow case (CNCL-(c)). The cases considered for the CFD study and the initial and boundary conditions used are shown in Table.2 and Table.5 respectively.

6. Validation of the 1-D model with the 3-D CFD numerical simulation

An exhaustive 3-D CFD study was performed to properly understand the dynamics and physics of the CNCL system for all the cases mentioned in Table.2. We shall now employ the CFD results to validate the 1-D semi-analytical model developed.

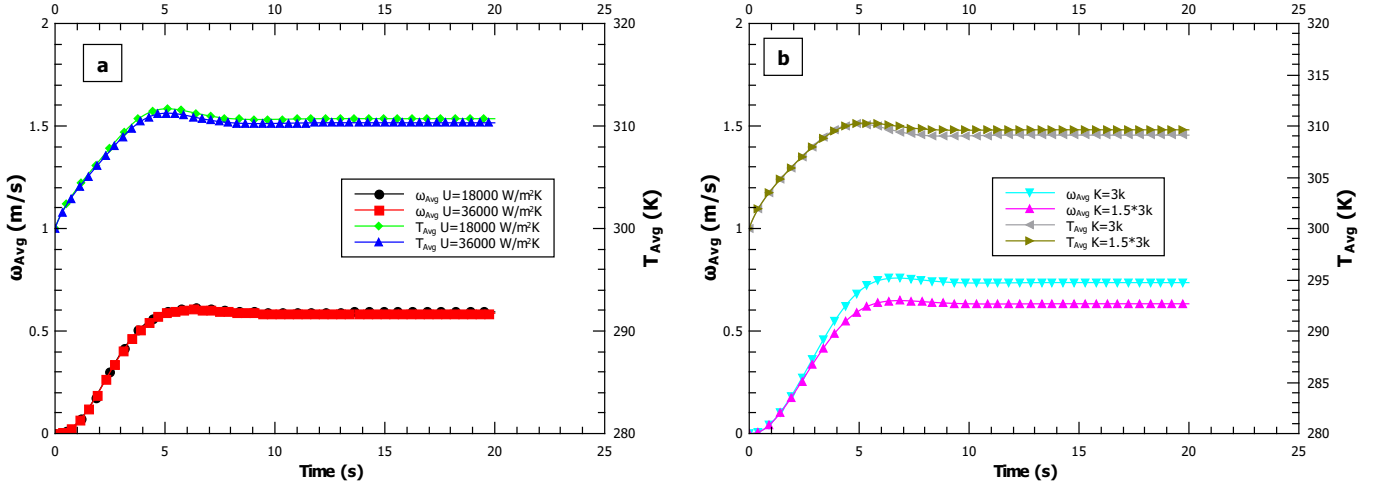


Figure 12: Sensitivity of the CNCL system dynamics to the magnitude of U and K .(a) Sensitivity w.r.t U (b) Sensitivity w.r.t K , $U=19000$.

The study conducted in section 5.4 indicates that the magnitude of heat transfer coefficient U for both the horizontal and vertical CNCL system lies in the range: 19,000-29,000 W/m^2K . The influence of variation of U on the CNCL system is studied and represented by Fig.12a and it indicates that the system dynamics is not greatly influenced by the heat transfer coefficient. Fig.12b indicates that the loop velocity of CNCL system is significantly affected by the variation in bend loss coefficient magnitude. The sensitivity of the CNCL system to the magnitude of the bend loss coefficient is significant when the Reynolds number of the system is lower, as at very low Reynolds number the value of ‘ K ’ is much greater than 1. Figure 4b shows that we can expect a $\pm 50\%$ error in 3K prediction, which explains the deviation presented in Table. 6.

To validate the CNCL 1-D model with 3-D CFD results, the length for 1-D model has to be equal to the length of the centerline axis minus two times the radius of curvature of the bend ($L = Y - 2R, L1 = X - 2R$). The bend length needs to be ignored as the bend loss coefficient takes into account the frictional effects and change in momentum at the bend. It is to be noted that this is only for a smooth 90° elbow bend considered for the present study. For other fittings the length has to be determined after accounting for the loss through the fitting. Thus for validating the present CFD study with 1-D model we employ $L = L1 = 1 - 2 \times 0.04 = 0.92 m$.

Table 6: Bend loss coefficient (K) used for validation of the 1-D model with CFD.

Case	Reynolds number at steady state	3K method prediction	K used for validation	% Deviation between 3K prediction and K used for validation
CNCL-(a)	2920	0.90	0.90	0
CNCL-(b) Loop 1	2920	0.90	0.90	0
CNCL-(b) Loop 2	524	2.16	1.1	49.07
CNCL-(c)	2348	0.97	0.97	0
CNCL-(d)	3160	0.88	0.88	0

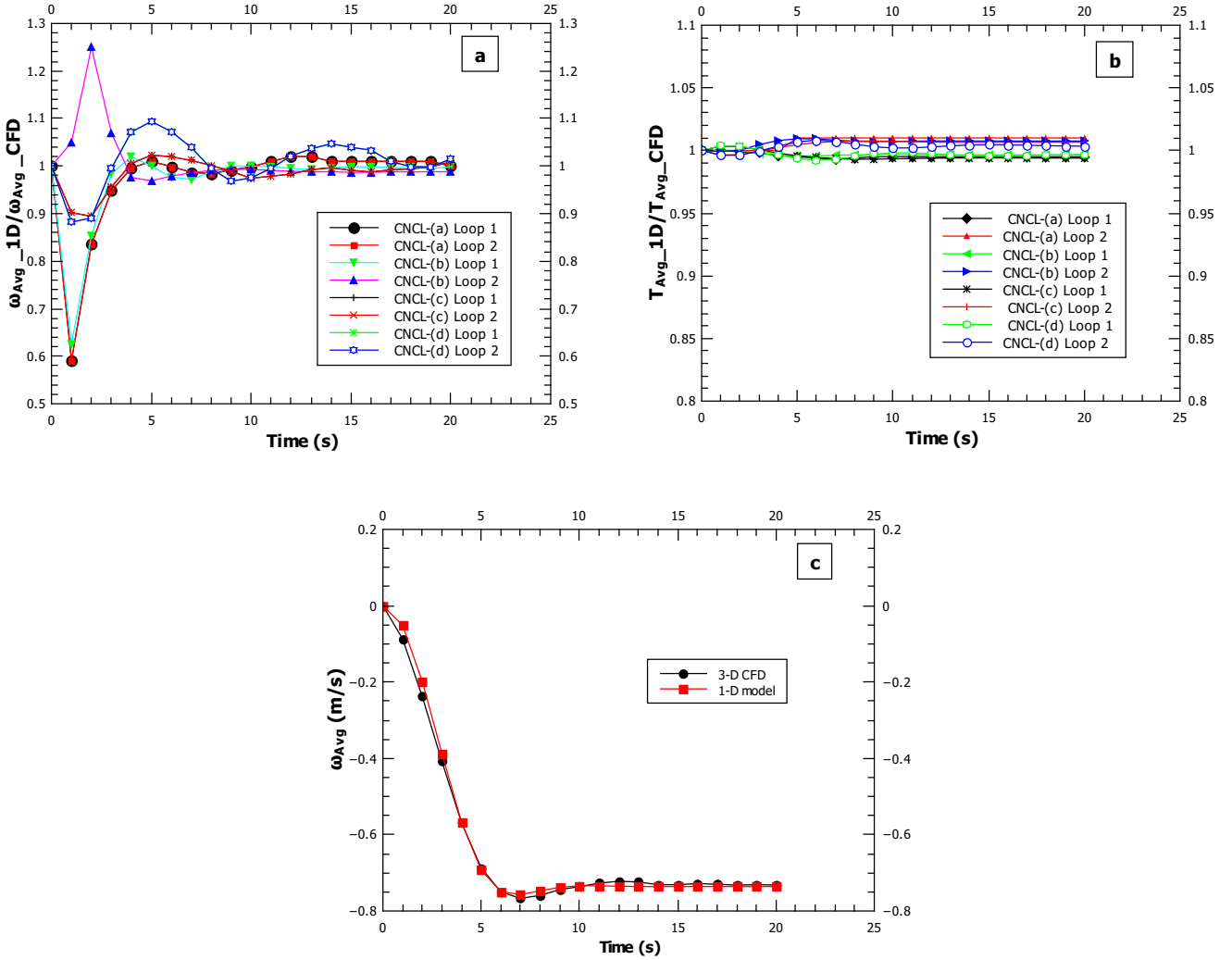


Figure 13: The validation of the 1-D CNCL model with 3-D CFD simulations are presented in the current figure. (a) The transient plot of ratio average velocity of 1D with CFD (b) Transient plot of ratio average temperature of 1D with CFD (c) Transient plot of the average velocity of 1D and CFD prediction of Loop 1 for case-CNCL-(a).

Figure 13 indicates a good agreement among the 3D CFD simulations and the 1-D semi-analytical model predictions with $\pm(2 - 3)\%$ error at steady state for velocity and $\pm 1\%$ error at steady state for average temperature. Figure 13a indicates that during the initial transience of velocity there is a huge deviation, this is because of the low magnitudes of velocity and because of the fully developed flow assumption at time $t = 0$ s (The transient nature of the friction factor in the developing region is not modeled). Figure 13c represents the comparison of transient velocity behavior of Loop 1 of CNCL-(a) (which corresponds to the case exhibiting maximum deviation during the initial transience behavior presented in Figure 13a), we can clearly see that there is a good agreement between 3-D CFD data and 1D model prediction.

7. Non-dimensionalization of the CNCL system

To perform a general study of the CNCL system and identify the non-dimensional numbers which characterize the CNCL system behavior, the system has been non-dimensionalized.

The non-dimensional CNCL system is represented by the following equations:

$$\frac{dRe_1}{d\zeta} = \left[Gr_1 \right] \oint (\theta_1) f(s) ds - \left[Co_1 \right] (Re_1)^{2-d} - \frac{nK}{4} (Re_1)^2 \quad (38)$$

$$\frac{d\theta_1}{d\zeta} + Re_1 \frac{d\theta_1}{ds} = \left[Fo_1 \right] \frac{d^2\theta_1}{ds^2} + h_1(s) - \left[St_1 \right] \delta(s) \left(\theta_1 - (1/Co_2)\theta_2 \right) \quad (39)$$

$$\frac{dRe_2}{d\zeta} = \left[Gr_2 \right] \oint (\theta_2) f(s) ds - \left[Co_1 \right] (Re_2)^{2-d} - \frac{nK}{4} (Re_2)^2 \quad (40)$$

$$\frac{d\theta_2}{d\zeta} + \left[\frac{\nu_2}{\nu_1} \right] Re_2 \frac{d\theta_2}{ds} = \left[Fo_2 \right] \frac{d^2\theta_2}{ds^2} + h_2(s) + \left[St_2 \right] \delta(s) \left(Co_2\theta_1 - \theta_2 \right) \quad (41)$$

where, $\theta_i = T_i - T_0/\Delta T_i$, $\zeta = t/t_0$, $s = x/x_0$, $t_0 = x_0 D_h/\nu_1$, $\Delta T_i = (4Q''t_0)/(\rho_i C p_i D_h)$, $x_0 = (L + L1)$ and the non-dimensional parameters are defined as follows:

$$Co_1 = \frac{2bx_0}{D_h} \quad (42)$$

$$Co_2 = \frac{\Delta T_1}{\Delta T_2} \quad (43)$$

$$Fo_i = \frac{\alpha_i t_{0,i}}{x_0^2} \quad (44)$$

$$St_i = \frac{U t_{0,i}}{\rho_i C p_i D_h} \quad (45)$$

$$Re_i = \frac{\omega_i D_h}{\nu_i} \quad (46)$$

$$Gr_i = \frac{g\beta_i \Delta T_i x_0 D_h t_{0,i}}{(L + L1)\nu_i} \quad (47)$$

From the above-mentioned equations, we can clearly see that Reynolds number, Grashof number, Fourier number, Stanton number, Co_1 and Co_2 determine the complete CNCL system behavior. A thorough parametric study is undertaken to understand the physics of the CNCL system considering the same fluid within the two loops. Considering same fluid in both loops leads to the following simplification $Gr_1 = Gr_2 = Gr$, $Fo_1 = Fo_2 = Fo$, $St_1 = St_2 = St$, $\Delta T_1 = \Delta T_2 \implies Co_2 = 1$. The simplified governing equations are represented as follows:

$$\frac{dRe_1}{d\zeta} = \left[Gr \right] \oint (\theta_1) f(s) ds - \left[Co_1 \right] (Re_1)^{2-d} - \frac{nK}{4} (Re_1)^2 \quad (48)$$

$$\frac{d\theta_1}{d\zeta} + Re_1 \frac{d\theta_1}{ds} = \left[Fo \right] \frac{d^2\theta_1}{ds^2} + h_1(s) - \left[St \right] \delta(s) \left(\theta_1 - \theta_2 \right) \quad (49)$$

$$\frac{dRe_2}{d\zeta} = \left[Gr \right] \oint (\theta_2) f(s) ds - \left[Co_1 \right] (Re_2)^{2-d} - \frac{nK}{4} (Re_2)^2 \quad (50)$$

$$\frac{d\theta_2}{d\zeta} + Re_2 \frac{d\theta_2}{ds} = \left[Fo \right] \frac{d^2\theta_2}{ds^2} + h_2(s) + \left[St \right] \delta(s) \left(\theta_1 - \theta_2 \right) \quad (51)$$

8. Results and Discussion

A detailed parametric study is undertaken to understand the physics of the CNCL system. The CNCL system containing the same fluid in its component loops is considered as it leads to symmetrical behavior of transient velocity and average temperature plots about the initial conditions when heater and cooler positions similar to cases CNCL-(a) to CNCL-(d) are used. This allows us to describe the complete CNCL system using $Re = \frac{|\omega_{1,2}|D_h}{\nu}$ and $\theta_{Avg} = |\theta_{Avg,1,2}|$ unless explicitly stated. For simplifying the specification of the heater-cooler location on both the vertical and horizontal CNCL systems we use the notation represented in Fig.14 from here onwards. In this study, we are solely interested in studying the effect of one heater and cooler per CNCL system.

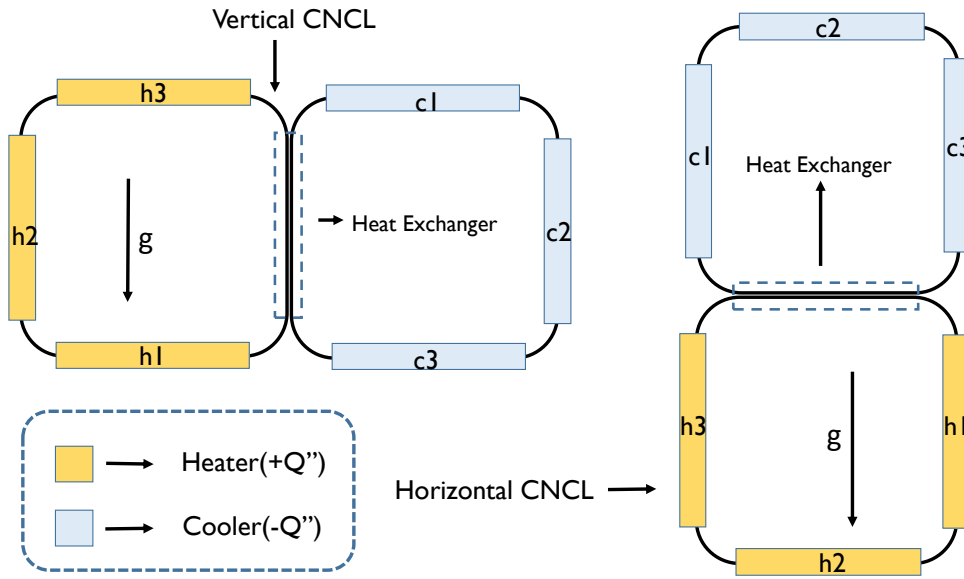


Figure 14: Heater and Cooler notations used for the current study. The configuration ‘Vertical CNCL h1c1’ refers to a vertical CNCL system where, only heater-‘h1’ and cooler-‘c1’ are switched on and the remaining heaters (‘h2’ and ‘h3’) and coolers (‘c2’ and ‘c3’) are set to $Q'' = 0 \text{ W/m}^2$. The horizontal CNCL system is obtained by rotating the vertical CNCL system anticlockwise w.r.t gravity as represented in the figure.

8.1. Comparison of vertical and horizontal CNCL systems

Figure 15 compares the horizontal and vertical CNCL systems for heater cooler configuration h1c1. We can observe a distinct difference in the behavior exhibited by the vertical and horizontal systems, as the heater h1 and cooler c1 are located on the horizontal legs (w.r.t gravity) of the vertical CNCL system (VCNCL) and on the vertical legs (w.r.t gravity) of the horizontal CNCL system (HCNCL).

The horizontal orientation of the heater and cooler on the VCNCL system implies that the energy supplied at the heater and cooler must propagate through conduction (within the fluid) to the vertical legs and only then can the buoyancy forces begin to act to drive the fluid within the loops of the system. This initial delay causes the vertical CNCL to have lesser oscillations in the ‘ Re vs ζ ’ plot and a higher θ_{Avg} at steady state.

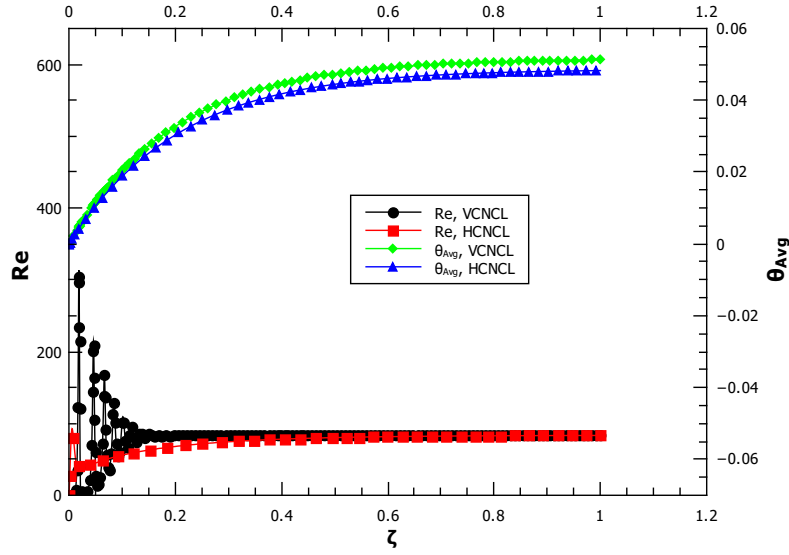


Figure 15: Comparison of transient behaviour of vertical and horizontal CNCL system for heater cooler arrangement h1c1 for $Gr=10^8$, $Fo=1$, $As=1$, $St=10$, $Co1=1000$.

8.2. Comparison of counter flow and parallel flow behavior

The HCNCL system with h2c2 heater cooler orientation is the only configuration where both the counter flow and parallel flow at the common heat exchanger section are exhibited just by changing the initial velocity conditions. The parallel flow configuration is obtained when the initial velocity at time $t = 0$ s is in positive direction in both Loop 1 and Loop 2 (i.e. both loops have clockwise velocity w.r.t origin ‘O’). The counter flow configuration can be obtained when the initial velocity at time $t = 0$ s is in the positive direction in Loop 1 and negative direction in Loop 2 (i.e. Loop 1 has clockwise velocity and Loop 2 has anti-clockwise velocity w.r.t origin ‘O’).

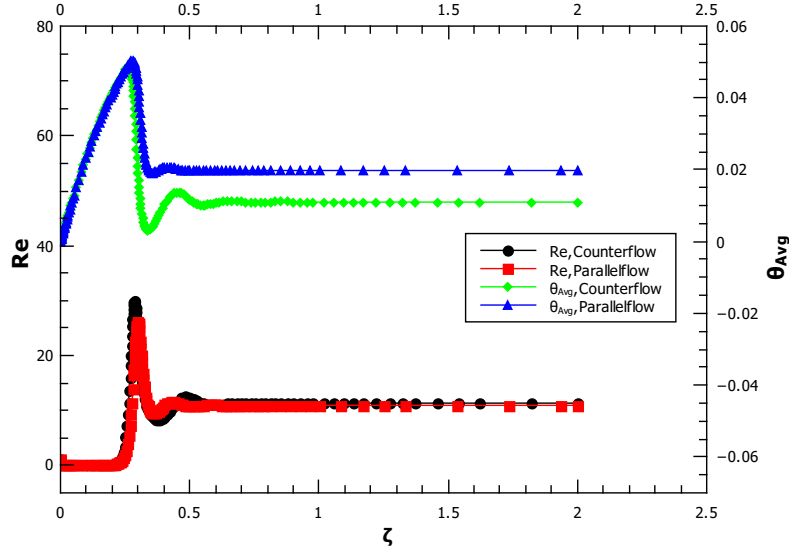


Figure 16: Effect of parallel and counter flow configurations on horizontal CNCL with h2c2 heater cooler configuration for $Gr=10^6$, $Fo=1$, $As=1$, $St=100$, $Co1=1000$.

From Fig.16 we observe that for the given conditions the steady state θ_{Avg} for counterflow is lower than parallel flow, this is because of the temperature distribution within the fluid at the common heat exchange section for Loop 1 and Loop 2. For both the counterflow and parallel flow conditions we observe from the ‘ Re vs ζ ’ plot that for the h2c2 heater cooler configuration, both the heater and cooler are on the horizontal legs (w.r.t gravity) of the HCNCL,

thus no flow is initiated until the energy is transferred to the vertical legs. This is the reason we can initialize the flow conditions to attain the parallel flow or counterflow arrangement at the common heat exchange section.

The non-dimensional average temperature for both counter and parallel flow condition increases at the same rate till the flow is initiated. After the flow is initiated by the buoyancy forces, the magnitude of θ_{Avg} begins to drop for both parallel and counter flow condition, thus the case which attains steady state quicker has a higher magnitude of θ_{Avg} . For the parallel flow condition the temperature difference between the hot and cold fluids along the flow direction decreases, but it is nearly constant for the counterflow condition. This implies that the heat transfer along the flow direction for parallel flow condition at the common heat exchange section decreases, while it is nearly constant along the flow direction for counterflow condition. This promotes a faster heat transfer rate for the parallel flow condition compared to the counterflow condition, which results in the parallel flow case attaining the steady state faster. This in turn leads to a larger magnitude of θ_{Avg} and lower value of Re for the parallel flow case compared to the counterflow case.

8.3. Effect of Grashof number on the CNCL system

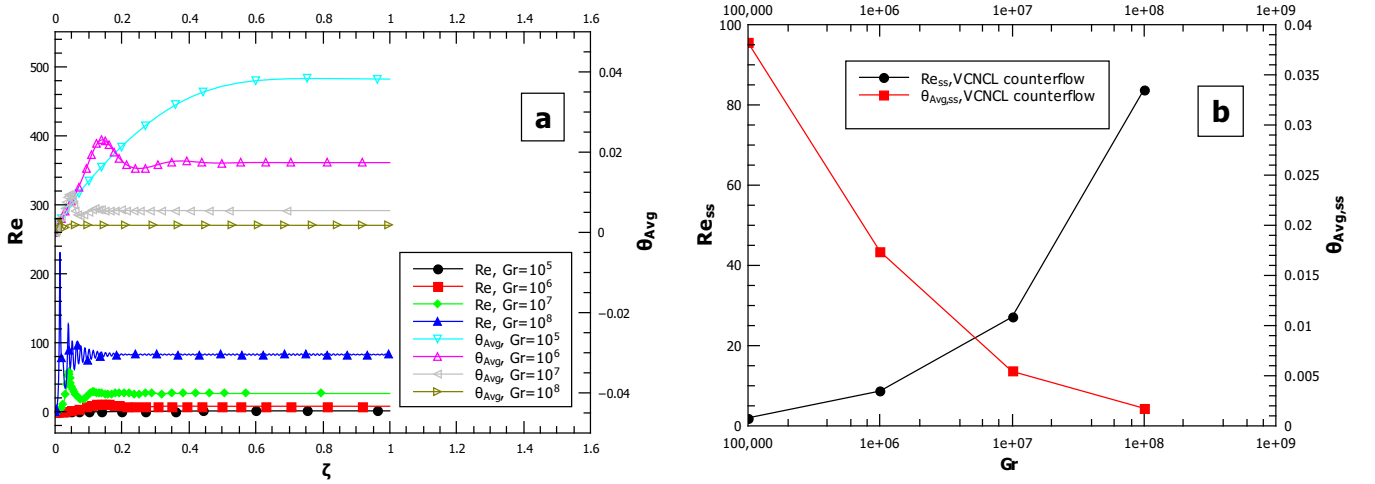


Figure 17: Effect of Grashof number (Gr) on the VCNCL system h1c1 configuration for $As=1, St=3000, Fo=1, Col=1000$.(a) Transient behaviour (b) Steady state trend.

From Fig.17a, we observe that with an increase in Grashof number the flow oscillations increase along with an increase in the steady-state Reynolds number and decrease in θ_{Avg} .

The flow in the component loops of the CNCL system is induced by $\oint(\theta_i)f(s)ds$, which represents the temperature distribution in the vertical legs (w.r.t gravity) of the CNCL system and determines the magnitude of the buoyancy forces ($Gr \oint(\theta_i)f(s)ds$).

With the increase in Grashof number, the magnitude of the buoyancy forces increases which push the fluid at a faster rate resulting in higher fluid velocity. The forces resulting from friction and momentum change at the bend act opposite the buoyancy force and try to restrain the fluid motion. Because the fluid is flowing at a faster rate within the loop, this leads to a quicker attainment of a temperature distribution along the loop such that the magnitude of $\oint(\theta_1)f(s)ds$ reduces which in-turn leads to the decrease in buoyancy forces. The decrease in buoyancy forces causes a decrease in the flow velocity and a simultaneous increase in the viscous forces (as it is inversely proportional to Re according to equation-11), which further tries to decrease the flow velocity. As the flow velocity drops, the temperature distribution ($\oint(\theta_1)f(s)ds$) increases leading to an increase in the buoyancy forces yet again. The process repeats itself

till all the forces balance each other, which satisfies the following condition:

$$Gr \oint (\theta_i) f(s) ds = Co_1 (Re_{i,ss})^{2-d} + \frac{nK}{4} (Re_{i,ss})^2 \quad (52)$$

This explains the oscillations observed in the 'Re vs ζ ' plot. Equation 54 explains why the magnitude of the steady-state Reynolds number increases with Gr .

Fig.17b depicts the steep rate of increase in Re and decrease in the rate of drop of θ_{Avg} with increasing Gr . The steep rate of increase in Re_{ss} is due to the steep decline in the viscous forces with increasing Reynolds number. Increase in Gr results from an increase in the magnitude of ΔT . Since $\theta_{Avg} \propto \frac{1}{\Delta T}$ with increasing Gr the magnitude of θ_{Avg} drops, this also explains the rate of drop of θ_{Avg} .

8.4. Effect of Fourier number on the CNCL system

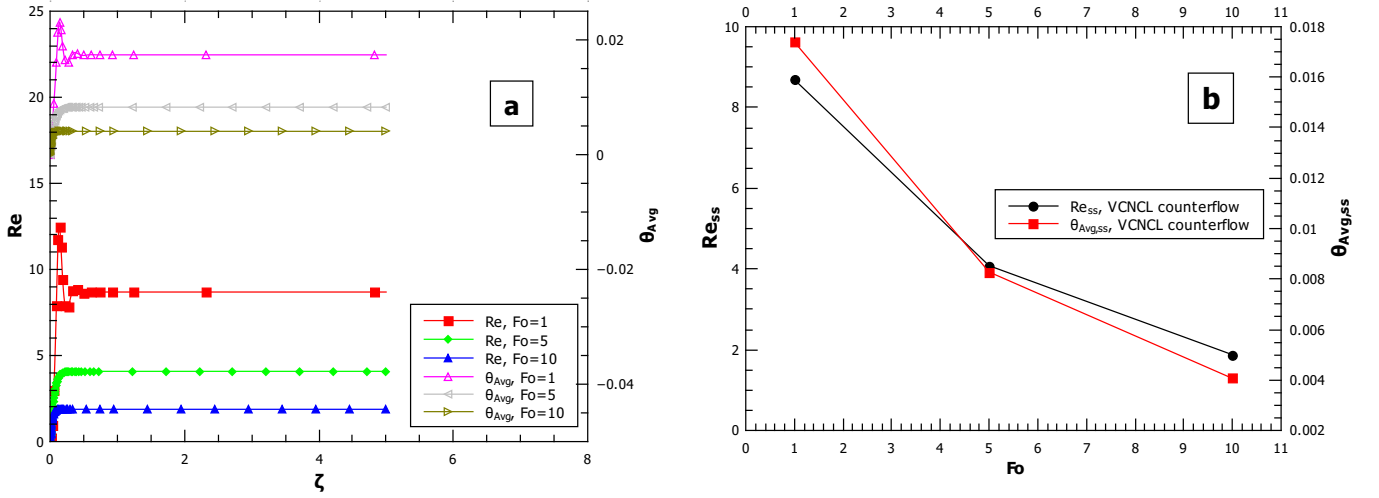


Figure 18: Effect of Fourier number (Fo) on the VCNCL system with h1c1 configuration for $Gr=10^6$, $St=3000$, $As=1$, $Co1=1000$.(a) Transient behaviour (b) Steady state trend.

From Fig.18a and Fig.18b we observe that both Re and θ_{Avg} decrease with increase in Fo . With the increase in Fo , we are effectively increasing the thermal diffusivity of the fluid considered for the study. With an increase in thermal diffusivity the temperature gradient across the entire CNCL system drops which leads to decrease in the buoyancy forces that drive the system. This explains the decrease in magnitude of Re with increasing Fo .

The increase in Fo can also be due to the increase in magnitude of t_0 which leads to an increase in ΔT . With rise in magnitude of ΔT the magnitude of θ_{Avg} decreases (as per the definition). This explains the decrease in θ_{Avg} with increasing Fo .

8.5. Effect of aspect ratio on the CNCL system

As of the CNCL is defined as :

$$As = \frac{L}{L1} \quad (53)$$

To understand the effect of variation of As ($0 < As \leq 1$) on the CNCL system, we assume $L1 = 1$ and $0 < L \leq 1$.

With the increase in the magnitude of As , the height of the VCNCL (L) increases which leads to the following effects:

1. An increase in the volume of fluid which is propelled by buoyancy forces represented by $D_h^2 \oint f(s) ds$.

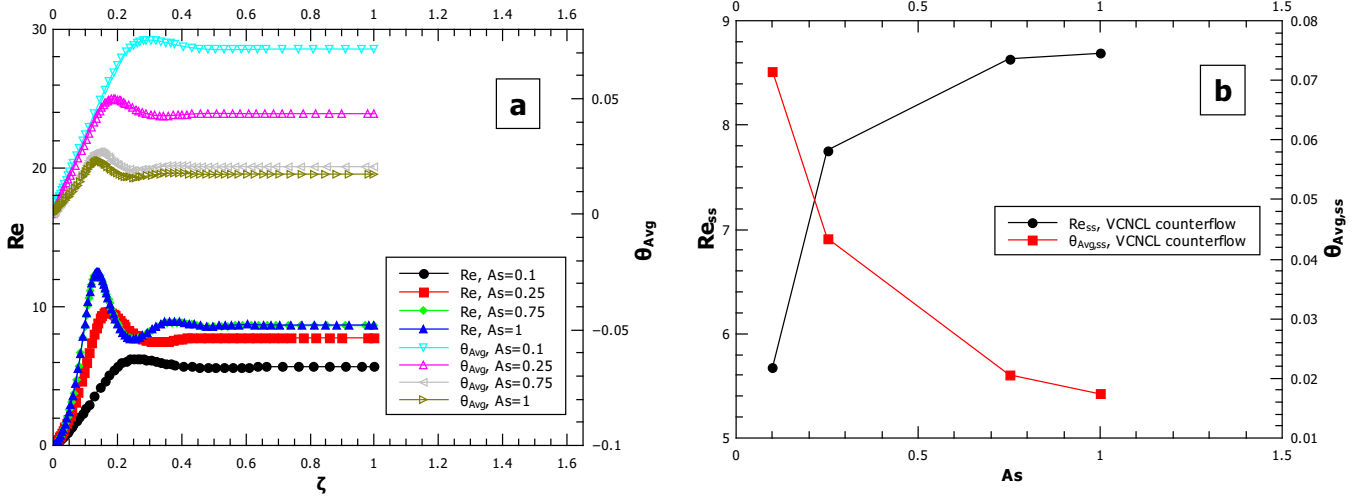


Figure 19: Effect of aspect ratio (As) on the VCNCL system h1c1 configuration for $Gr=10^6$, $St=3000$, $Fo=1$, $Co1=1000$.(a) Transient behaviour (b) Steady state trend.

2. An increase in the length ($2x_0$) of the component loops of the CNCL which results in an increase in Co_1 and Gr both of which are directly proportional to x_0 . This leads to an increase in the viscous forces ($Co_1 Re^{2-d}$) and buoyancy forces ($Gr \oint(\theta_1) f(s) ds$). With an increase in x_0 the Fourier number decreases which results in an increase in $\oint(\theta_1) f(s) ds$ that leads to lesser uniformity in temperature across the loop.
3. An overall increase in the volume of the system: $2D_h^2 x_0$. This results in an increase in the thermal inertia of the system, causing the system to resist change in θ_{Avg} . This along with the fact that $\theta_{Avg} \propto \frac{1}{x_0}$ explains the decrease in magnitude with increase in As .
4. An increase in the area of the common heat exchange section of the VCNCL system. This results in an increase in the rate of heat transfer leading to faster attainment of steady state for θ_{Avg} as observed in Fig.19a.
5. From equation 56 we can infer that although the magnitude of θ_{Avg} decreases the magnitude of buoyancy forces has to be relatively greater than the viscous forces, which results in the increase in Re with increase in As and the rate of drop of slope of Re vs As as observed in Fig.19b can be attributed to the reduction in the rate of increase in buoyancy forces relative to viscous forces.

$$Gr(\uparrow) \left(\oint(\theta_1) f(s) ds(\uparrow) \right) = Co_1 (Re_{1,ss})^{2-d}(\uparrow) + \frac{nK}{4} (Re_{1,ss})^2 \quad (54)$$

The As of a system is a complex parameter, as any change in its value effects all the other parameters of the CNCL system. Thus it is difficult to gauge the effect of variation of As on the system behavior.

8.6. Effect of Stanton number on the CNCL system

As observed in Fig.20 we notice that varying the magnitude of St does not affect the transient and steady-state behavior significantly at least for the parameters considered for the study. This study corroborates the sensitivity study of the CNCL system considered in Fig.12. This leads us to conclude that the correlations used to predict the heat transfer need not be very precise to give a decent prediction of the CNCL behavior.

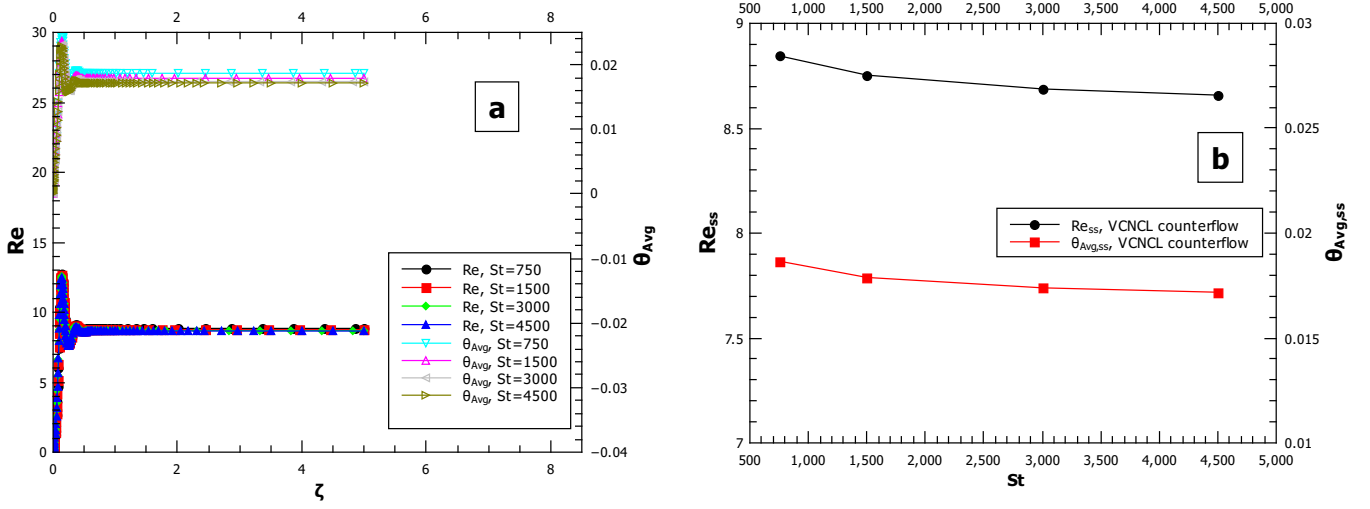


Figure 20: Effect of Stanton number (St) on the CNCL system for $Gr=10^6$, $Fo=1$, $As=1$, $Co1=1000$.(a) Transient behaviour (b) Steady state trend.

8.7. Effect of $Co1$ on the CNCL system

From Fig.21 we observe that with an increase in $Co1$ the magnitude of Re drops, while the magnitude of θ_{Avg} rises. From Fig.21a, we also observe the decrease in the oscillatory behavior exhibited by the CNCL system. With the increase in $Co1$ the magnitude of viscous forces increases relative to the buoyancy forces which explains the decrease in the magnitude of Re . As the velocity in the loop decreases, the temperature drop across the heating and cooling section increases which leads to an increase in the magnitude of θ_{Avg} with increasing $Co1$.

$$(Gr \oint (\theta_1) f(s) ds)(constant) = Co_1 (Re_{1,ss})^{2-d}(\uparrow) + \frac{nK}{4} (Re_{1,ss})^2 \quad (55)$$

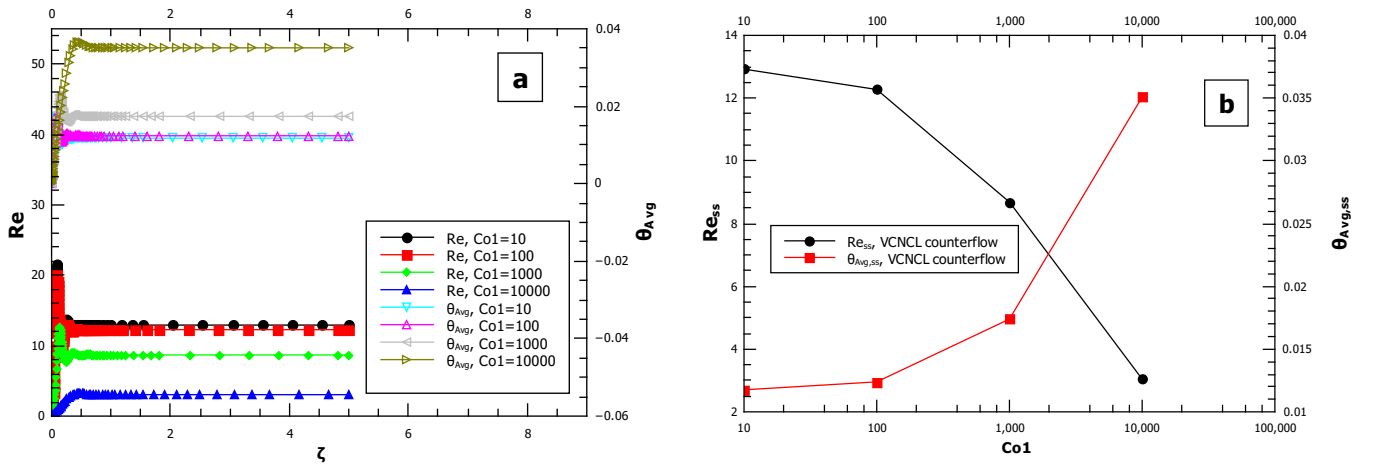


Figure 21: Effect of Geometric factor ($Co1$) on the VCNCL system with h1c1 configuration for $Gr=10^6$, $Fo=1$, $As=1$, $St=3000$.(a) Transient behaviour (b) Steady state trend.

8.8. Effect of initial conditions on the CNCL system

The initial condition of the CNCL system which can be changed is $Re(\zeta = 0)$. From Fig.22 we observe that the transient behavior of the VCNCL system is largely unaffected by the variation in initial conditions. From Fig.22a it is to be noted that any transience associated with is $Re(\zeta = 0)$ dies out very quickly and the VCNCL system response remains unaltered.

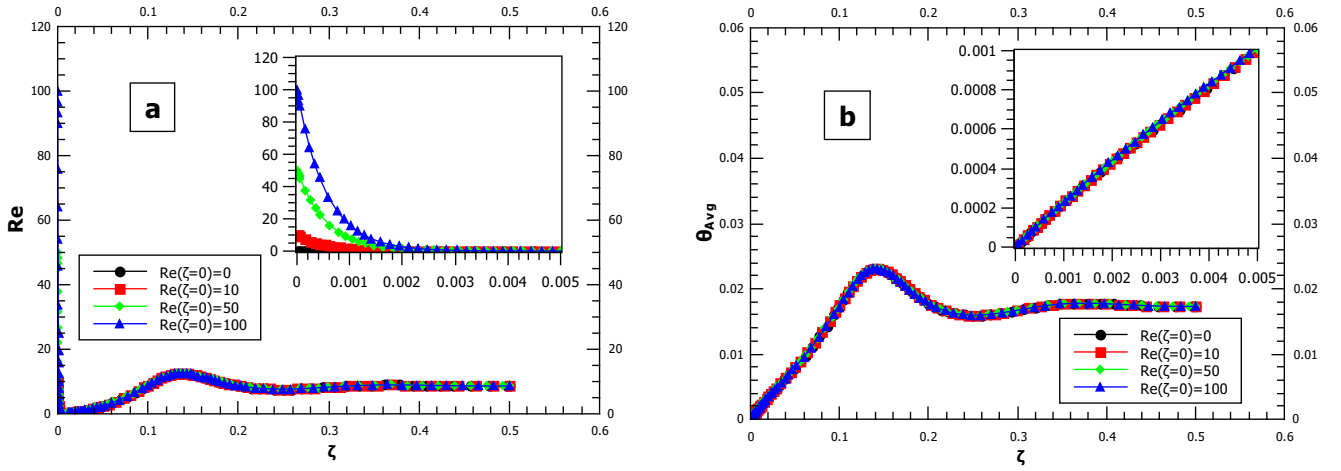


Figure 22: Effect of initial velocity represented by $Re(\tau = 0)$ on the VCNCL system with h1c1 configuration for $Gr=10^6$, $Fo=1$, $As=1$, $St=3000$, $Co1=1000$.(a) Transient behaviour (b) Steady state trend.The inset graphs represent the transient behaviour of the respective plots for $\zeta \rightarrow (0 - 0.005)$.

8.9. Effect of parallel flow vs counter flow arrangement at the heat exchanger section of HCNCL system

The horizontal CNCL system with h2c2 heater cooler configuration is the only condition which can exhibit both counter and parallel flow arrangement at the common heat exchanger section of the CNCL system. This is because for the h2c2 configuration of the HCNCL system all the energy transfer in the CNCL system occurs on the horizontal legs of the component loops. This implies that the buoyancy forces generated at the heat transfer sections does not dictate the flow direction. Thus by choosing appropriate initial flow conditions as described in section 8.2, the parallel flow or counter flow can be induced within the HCNCL system by directing the heated or cooled fluid sections to the vertical legs of the system.

Table 7: Values of non-dimensional numbers utilised for the parametric study of HCNCL system.

Figure	Gr	As	Fo	St	Co1
Fig.22(a)	$10^5 \rightarrow 10^8$	1	1	3000	1000
Fig.22(b)	10^6	$0.1 \rightarrow 1$	1	3000	1000
Fig.22(c)	10^6	1	$1 \rightarrow 10$	3000	1000
Fig.22(d)	10^6	1	1	$750 \rightarrow 4500$	1000
Fig.22(e)	10^6	1	1	3000	$10 \rightarrow 10^4$

For all the other heater cooler positions for both the HCNCL and VCNCL systems atleast one of the heat transfer sections is vertical w.r.t gravity and the buoyancy forces generated there determine the flow direction irrespective of the initial flow conditions.

Table.7 indicates the ranges in which parametric studies were conducted on the HCNCL system for different non-dimensional parameters. The only difference between the parallel flow and counter flow systems is the temperature distribution at the common heat exchanger section of the CNCL system, which leads to a difference in trends observed in Fig.23.

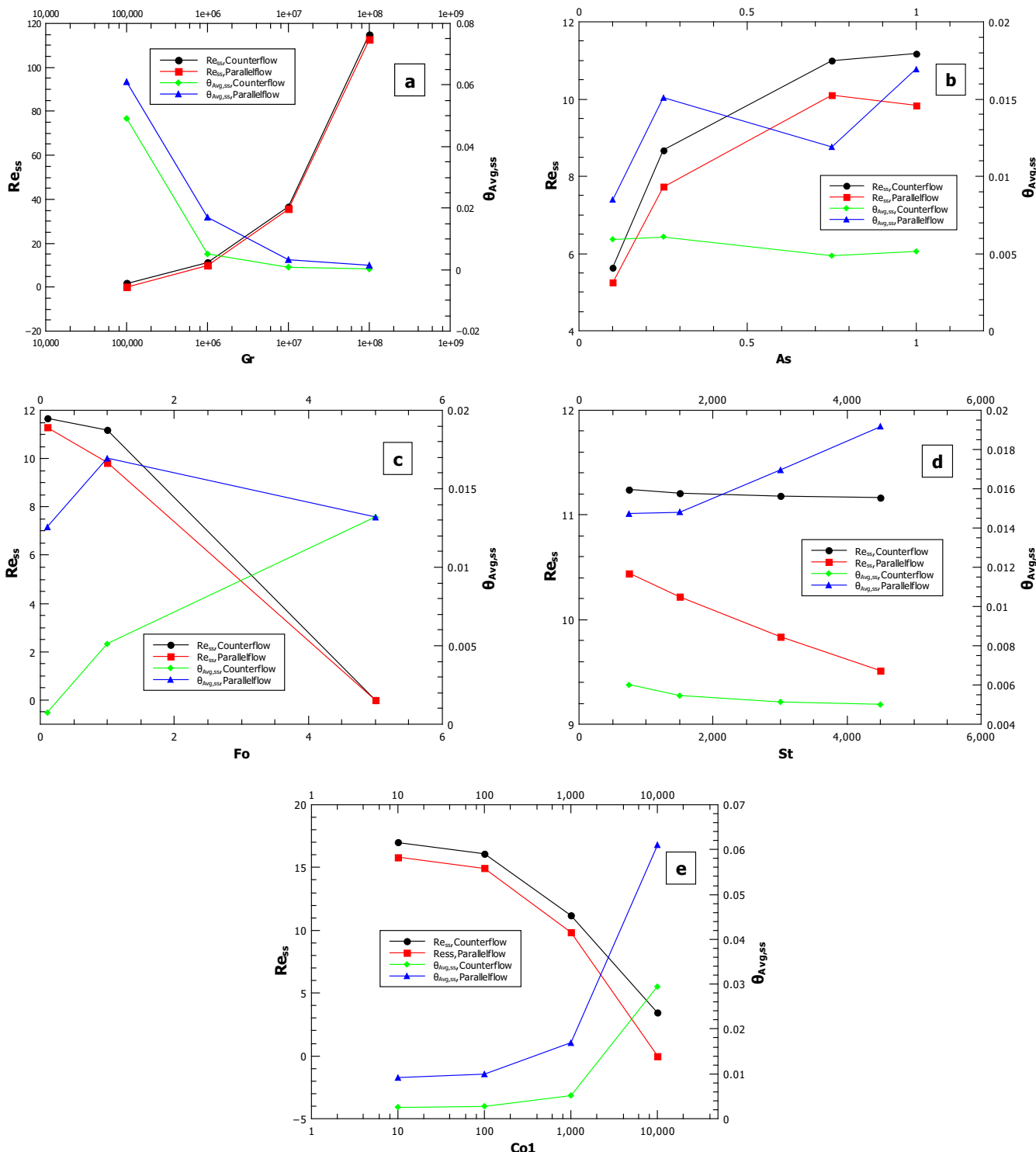


Figure 23: Parametric study of the parallel and counterflow configurations of horizontal CNCL system with h2c2 heater cooler configuration. The values of the non-dimensional numbers considered are listed in Table.7.

8.10. Effect of heater cooler configuration on the CNCL system

A transient and steady-state analysis on the effect of the heater and cooler location on the CNCL dynamics of both horizontal and vertical systems is presented.

8.10.1. Effect of heater cooler configuration on the vertical CNCL system

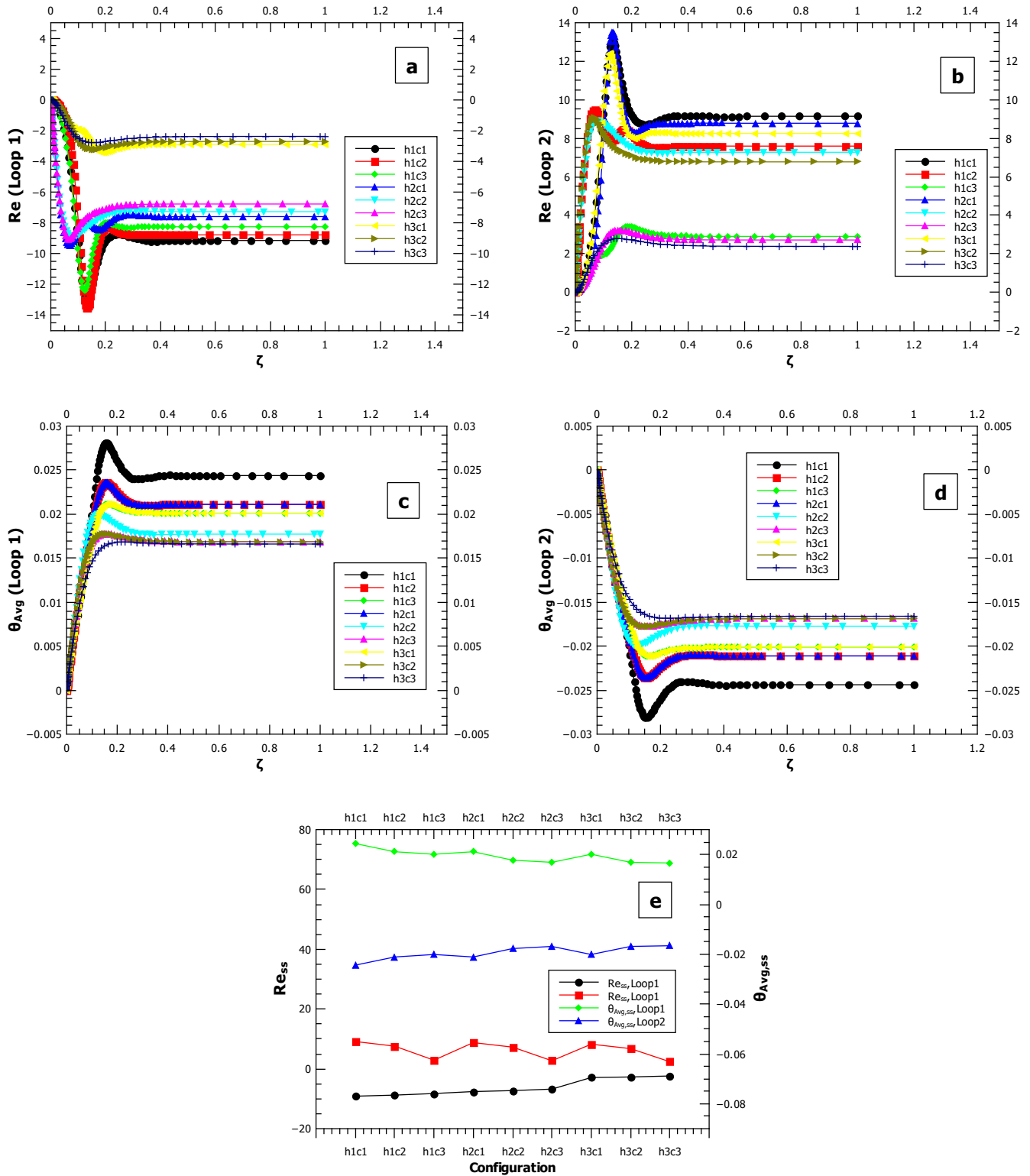


Figure 24: Effect of heater cooler orientation on the Vertical CNCL system for $Gr=10^6$, $Fo=1$, $As=1$, $St=100$, $Co1=1000$.

The following observations can be made from Fig.24 :

1. The magnitude of θ_{Avg} for all the heater-cooler configurations at steady state is symmetric about $\theta_{Avg}(\zeta = 0)$ (which is equal to zero). This implies $\theta_{Avg,1,ss}/\theta_{Avg,2,ss} = 1$.
2. The magnitude of Re_{ss} is not equal in the component loops of the VCNCL system for all the heater cooler configurations.
3. Table.8 presents the ratio of Reynolds numbers of Loop 1 to Loop 2 at steady state. We observe that only for h1c1, h2c2, h3c3 configurations do we have symmetric transient and steady state behavior. The negative sign denotes that the flow arrangement at the common heat exchanger is counterflow.
4. From table.8 we also observe that :

$$\frac{Re_{1,ss}(hicj)}{Re_{2,ss}(hicj)} \times \frac{Re_{1,ss}(hjci)}{Re_{2,ss}(hjci)} = 1 \quad (56)$$

where 'i','j' represent the position of the heater and cooler for the 'hicj' configuration.

5. All the heater-cooler configurations of the VCNCL system exhibit counterflow condition at the common heat exchanger section for all stable convective flow cases.
6. h1c1 configuration corresponds to the maximum magnitude of Re_{ss} and θ_{Avg} and the h3c3 configuration corresponds to the minimum values of the same parameters for the vertical CNCL system respectively.

Table 8: Ratio of $\left(\frac{Re_{1,ss}}{Re_{2,ss}}\right)$ of the VCNCL system for all heater cooler configurations.

	c1	c2	c3
h1	-1	-1.15	-2.85
h2	-1/1.15	-1	-2.5
h3	-1/2.85	-1/2.5	-1

8.10.2. Effect of heater cooler configuration on the horizontal CNCL system

For the study of heater cooler configuration of the HCNCL system, all configurations apart from h2c2 are studied. The h2c2 configuration of the HCNCL system is peculiar as it exhibits both parallel and counter flow depending on the initial conditions.

The following observations can be made from Fig.25:

1. The magnitude of θ_{Avg} for all the heater-cooler configurations at steady state is symmetric about $\theta_{Avg}(\zeta = 0)$, which is equal to zero. This implies $\theta_{Avg,1,ss}/\theta_{Avg,2,ss} = 1$.
2. The HCNCL systems shifts between the parallel flow and counter flow configuration depending on the heater cooler location on the HCNCL system.
3. The magnitude of Re_{ss} is not equal in the component loops of the HCNCL system for all the heater cooler configurations.
4. Table.9 presents the ratio of Reynolds numbers of Loop 1 to Loop 2 at steady state. The sign denotes whether the flow arrangement at the common heat exchanger is parallel flow or counterflow. Negative sign denotes the counterflow arrangement.
5. From table.9 we also observe that :

$$\frac{Re_{1,ss}(hicj)}{Re_{2,ss}(hicj)} \times \frac{Re_{1,ss}(hjci)}{Re_{2,ss}(hjci)} = 1 \quad (57)$$

where 'i','j' represent the position of the heater and cooler for the 'hicj' configuration.

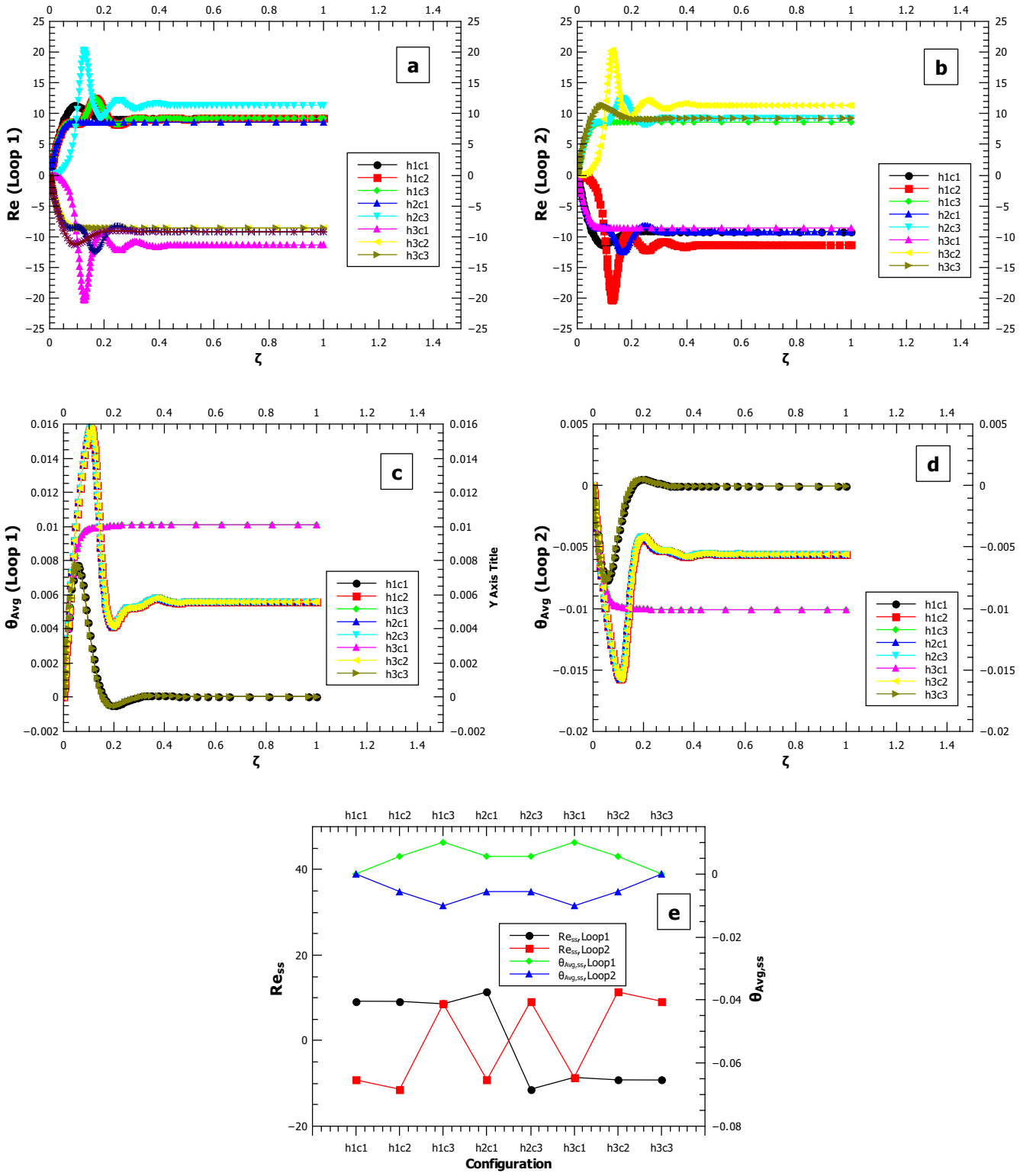


Figure 25: Effect of heater cooler orientation on the Horizontal CNCL system for $Gr=10^6$, $Fo=1$, $As=1$, $St=100$, $Co1=1000$.

Table 9: Ratio of $\left(\frac{Re_{1,ss}}{Re_{2,ss}}\right)$ of the HCNCL system for all heater cooler configurations.

	c1	c2	c3
h1	-1	-0.81	1
h2	-1/0.81	± 1	-1.24
h3	1	-1/1.24	-1

9. Conclusions

Thus far, the literature available on transient single-phase CNCL systems has been focused only on studying simple point contact CNCL which are of little practical value for industrial and engineering requirements. Thus to bridge this gap and fulfill the chosen objectives a 1-D single phase semi-analytical method to model the transient CNCL system having flat plate heat exchanger formed via the coupling of constituent square NCLs which have a square cross-section is proposed. To validate the proposed 1-D model a 3-D transient study is carried out using ANSYS Fluent 16.1 after the grid and time-step independence is established and the CFD methodology is validated. The CNCL with flat plate heat exchanger section is studied for both the vertical and horizontal configurations, thus ensuring a thorough and in-depth study. The following conclusions can be drawn from the present work:

1. The 1-D model of the CNCL system is an ideal tool that greatly minimizes the time required to understand the physics of the system, and it is robust enough to handle all the possible heat transfer boundary conditions (constant temperature, heat flux and volumetric heat generation), transient heat inputs and heat loss to the ambient surroundings. The 1-D model accurately predicts the trend of the CNCL system with minimal computational effort, thus the current work greatly simplifies and aids in the design of the CNCL system. Table.10 provides a qualitative comparison of the time taken for the 3-D CFD study vs 1-D semi-analytical model.

Table 10: Qualitative comparison of the time required for each of the parameters for a 3-D CFD case vs 1-D semi-analytical model.

Parameter under consideration	3-D CFD Study	1-D semi analytical model
Geometry creation	minimal	not required
Structured mesh generation	substantial	not required
Case setup	substantial	minimal
Simulation	significantly large	minimal
Post processing	significantly large	substantial
Grid and time step independence	significantly large	minimal

2. The non-dimensional numbers - $Gr, Re, St, Fo, Co1, Co2$ and As - determine the transient dynamics of the CNCL system.
3. The heater and cooler configurations on both the horizontal and vertical CNCL systems effect the system behavior significantly and the following equation represents the correlation of steady state Reynolds numbers of the component loops of the CNCL system:

$$\frac{Re_{1,ss}(hicj)}{Re_{2,ss}(hicj)} \times \frac{Re_{1,ss}(hjci)}{Re_{2,ss}(hjci)} = 1 \quad (58)$$

where 'i', 'j' represent the position of the heater and cooler for the 'hicj' configuration.

4. The vertical CNCL always exhibits counterflow arrangement at the common heat exchanger section for all the heater and cooler configurations, but the horizontal CNCL shuffles between the counter and parallel flow depending on the heater-cooler configuration for stable convective flows.
5. The horizontal CNCL with h2c2 heater cooler configuration is the only CNCL system which can exhibit both counter and parallel flow condition at the common heat exchanger section by setting the appropriate initial flow conditions.
6. The CNCL system seems to be very mildly sensitive to the variation in Stanton number, implying that even an un-precise heat transfer correlation can be considered to model the coupling with reasonable accuracy.

7. The limitation of the current modeling approach is that it does not take the wall effects into consideration. This may lead to deviation in the transient prediction, but by modifying the Stanton number to incorporate the conjugate, accurate steady state results can be obtained.
8. The study of chaotic CNCL systems is not considered in the present study and will be part of the future work.

Nomenclature

$T_{1,Avg}$	Circuit average temperature of loop 1 (K)
$T_{2,Avg}$	Circuit average temperature of loop 2 (K)
L	CNCL height used for 1-D model (m)
Y	CNCL height used for CFD study (m)
$L1$	CNCL width used for 1-D model (m)
X	CNCL width used for CFD study (m)
x	Distance from origin 'O' (m)
ω_1	Fluid velocity of loop 1 (m/s)
ω_2	Fluid velocity of loop 2 (m/s)
g	Gravitational constant (m/s^2)
Q''	Heat flux (W/m^2)
Q''_{CHX}	Heat transfer across the common heat exchanger section (W/m^2)
D_h	Hydraulic diameter of both loop 1 & 2 (m)
n	No of bends on the component NCL of the CNCL system
R	Radius of curvature of the bend (m)
U	Overall heat transfer coefficient at the heat exchanger section (W/m^2K)
T_0	Reference temperature of loop 1 & 2 (K)
C_p	Specific heat capacity (J/KgK)
a	Thermal diffusivity (m^2/s)
T_1	Temperature of Loop 1 (K)
T_2	Temperature of Loop 2 (K)
t	Time (s)

Greek letters

β	Coefficient of thermal expansion ($1/K$)
ρ	Density (kg/m^3)
ν	Kinematic viscosity (m^2/s)
ρ_0	Reference density (kg/m^3)
κ	Thermal conductivity ($W/(mK)$)
τ	Wall shear stress exerted on fluid (Pa)

Non-dimensional numbers

K	Bend losses coefficient ($K = \Delta P_{bend}/(\frac{1}{2}\rho\omega_i^2)$)
f_F	Fanning friction factor ($f_F = \tau_i/(\frac{1}{2}\rho\omega_i^2) = b/Re^d$)
Gr_m	Modified Grashof number ,Vijayan(2002) [19]
N_g	Geometric parameter ,Vijayan(2002) [19]

Constants

t_0	($t_0 = x_0 D_h / \nu_1$)
ΔT	($\Delta T_i = (4Q''t_0) / (\rho_i C_{p_i} D_h)$)
x_0	($x_0 = (L + L1)$)
b	14.23 (for fully developed flow in laminar regime)
d	1 (for fully developed flow in laminar regime)

Non dimensional parameters

Re	Reynolds number ($Re_i = \frac{\omega_i D_h}{\nu_i}$)
Gr	Grashof number ($Gr_i = \frac{g \beta_i \Delta T_i x_0 D_h t_{0,i}}{(L+L1) \nu_i}$)
Fo	Fourier number ($Fo_i = \frac{\alpha_i t_{0,i}}{x_0^2}$)
St	Stanton number ($St_i = \frac{U t_{0,i}}{\rho_i C_{p_i} D_h}$)
$Co1$	Non dimensional constant 1 ($Co1 = \frac{2bx_0}{D_h}$)
$Co2$	Non dimensional constant 2 ($Co2 = \frac{\Delta T_1}{\Delta T_2}$)
θ	Non dimensional temperature ($\theta_i = T_i - T_0 / \Delta T_i$)
ζ	Non dimensional time ($\zeta = t / t_0$)
s	Non dimensional length ($s = x / x_0$)

Subscripts

0	Any parameter at time $t = 0$ s
1	Any parameter referring to Loop 1
2	Any parameter referring to Loop 2
ss	Any parameter considered at steady state
Avg	Average value of the parameter
i	Refers to subscript '1' or subscript '2' according to relevance

Abbreviations

CFD	Computational Fluid Mechanics
$CNCL$	Coupled Natural Circulation Loop
$HCNCL$	Horizontal Coupled Natural Circulation Loop
NCL	Natural Circulation Loop
$PRHRS$	Passive Residual Heat Removal system
$VCNCL$	Vertical Coupled Natural Circulation Loop

10. References

References

- [1] D. N. Basu, S. Bhattacharyya, P. Das, A review of modern advances in analyses and applications of single-phase natural circulation loop in nuclear thermal hydraulics, *Nuclear Engineering and Design* 280 (2014) 326–348.
- [2] S. H. Davis, M. N. Roppo, Coupled Lorenz oscillators, *Physica D. Nonlinear Phenomena* 24 (1-3) (1987) 226–242.
- [3] P. Ehrhard, Dynamisches Verhalten der naturkonvektion in geschlossenen kreislaeufen, Ph.D. thesis, kfk-4373 (April 88) Dissertation, Universitaet Karlsruhe (1988).
- [4] O. Salazar, M. Sen, E. Ramos, Flow in conjugate natural circulation loops, *Journal of Thermophysics and Heat Transfer* 2 (2) (1988) 180–183.
- [5] X. Zhang, D. Lu, C. Guo, Analysis on transient response of natural circulation in coupled lbe loops, *Atomic Energy Science and Technology* 3 (2015) 013.
- [6] R. Duffey, D. Hughes, 16 - the safety of advanced reactors, in: I. L. Piro (Ed.), *Handbook of Generation IV Nuclear Reactors*, Woodhead Publishing Series in Energy, Woodhead Publishing, 2016, pp. 455 – 540.
- [7] P. Vijayan, M. Sharma, D. Saha, Steady state and stability characteristics of single-phase natural circulation in a rectangular loop with different heater and cooler orientations, *Experimental Thermal and Fluid Science* 31 (8) (2007) 925–945.
- [8] A. Fichera, A. Pagano, Modelling and control of rectangular natural circulation loops, *International journal of heat and mass transfer* 46 (13) (2003) 2425–2444.
- [9] P. Welander, On the oscillatory instability of a differentially heated fluid loop, *Journal of Fluid Mechanics* 29 (1) (1967) 17–30.
- [10] J. E. Hart, A new analysis of the closed loop thermosyphon, *International journal of heat and mass transfer* 27 (1) (1984) 125–136.
- [11] A. Rodríguez-Bernal, E. S. Van Vleck, Diffusion induced chaos in a closed loop thermosyphon, *SIAM Journal on Applied Mathematics* 58 (4) (1998) 1072–1093.
- [12] J. Y. Kudariyawar, A. M. Vaidya, N. K. Maheshwari, P. Satyamurthy, Computational study of instabilities in a rectangular natural circulation loop using 3d cfd simulation, *International Journal of Thermal Sciences* 101 (2016) 193–206.
- [13] W. F. Louissos, D. L. Hitt, C. M. Danforth, Chaotic flow in a 2d natural convection loop with heat flux boundaries, *International Journal of Heat and Mass Transfer* 61 (2013) 565–576.
- [14] A. C. Yunus, J. M. Cimbala, *Fluid mechanics fundamentals and applications*, International Edition, McGraw Hill Publication 185201.
- [15] R. Darby, R. P. Chhabra, R. Darby, *Chemical engineering fluid mechanics*, revised and expanded, CRC Press, 2001.
- [16] M. Edwards, M. Jadallah, R. Smith, Head losses in pipe fittings at low reynolds numbers, *Chemical Engineering Research and Design* 63 (1) (1985) 43–50.

- [17] N. Crawford, G. Cunningham, S. Spence, An experimental investigation into the pressure drop for turbulent flow in 90 elbow bends, *Proceedings of the Institution of Mechanical Engineers, Part E: Journal of Process Mechanical Engineering* 221 (2) (2007) 77–88.
- [18] A. Borgohain, B. Jaiswal, N. Maheshwari, P. Vijayan, D. Saha, R. Sinha, Natural circulation studies in a lead bismuth eutectic loop, *Progress in nuclear energy* 53 (4) (2011) 308–319.
- [19] P. Vijayan, Experimental observations on the general trends of the steady state and stability behaviour of single-phase natural circulation loops, *Nuclear Engineering and Design* 215 (1-2) (2002) 139–152.